

The MerR-family regulator NmlR is involved in the defense against oxidative stress in *Streptococcus pneumoniae*

Verena Nadin Fritsch ¹ | Nico Linzner ¹ | Tobias Busche ^{2,3} | Nelly Said ⁴ |
Christoph Weise ⁵ | Jörn Kalinowski ² | Markus C. Wahl ^{4,6} | Haike Antelmann ¹

¹Institute of Biology-Microbiology, Freie Universität Berlin, Berlin, Germany

²Center for Biotechnology, University Bielefeld, Bielefeld, Germany

³NGS Core Facility, Medical School OWL, Bielefeld University, Bielefeld, Germany

⁴Laboratory of Structural Biochemistry, Freie Universität Berlin, Berlin, Germany

⁵Institute of Chemistry and Biochemistry, Freie Universität Berlin, Berlin, Germany

⁶Macromolecular Crystallography, Helmholtz-Zentrum Berlin für Materialien und Energie, Berlin, Germany

Correspondence

Haike Antelmann, Institute for Biology-Microbiology, Freie Universität Berlin, Königin-Luise-Straße 12-16, D-14195 Berlin, Germany.
Email: haike.antelmann@fu-berlin.de

Funding information

Deutsche Forschungsgemeinschaft, Grant/Award Number: SFB973/ C08 (to H.A.), SPP1710/ AN746/4-1 and AN746/4-2 (to H.A.), TR84/ B06 (to H.A.) and WA1126/11-1 (project number 433623608) to M.C.W.

Abstract

Streptococcus pneumoniae has to cope with the strong oxidant hypochlorous acid (HOCl), during host-pathogen interactions. Thus, we analyzed the global gene expression profile of *S. pneumoniae* D39 towards HOCl stress. In the RNA-seq transcriptome, the NmlR, SifR, CtsR, HrcA, SczA and CopY regulons and the *etrx1-ccdA1-msrAB2* operon were most strongly induced under HOCl stress, which participate in the oxidative, electrophile and metal stress response in *S. pneumoniae*. The MerR-family regulator NmlR harbors a conserved Cys52 and controls the alcohol dehydrogenase-encoding *adhC* gene under carbonyl and NO stress. We demonstrated that NmlR senses also HOCl stress to activate transcription of the *nmlR-adhC* operon. HOCl-induced transcription of *adhC* required Cys52 of NmlR in vivo. Using mass spectrometry, NmlR was shown to be oxidized to intersubunit disulfides or S-glutathionylated under oxidative stress in vitro. A broccoli-FLAP-based assay further showed that both NmlR disulfides significantly increased transcription initiation at the *nmlR* promoter by RNAP in vitro, which depends on Cys52. Phenotype analyses revealed that NmlR functions in the defense against oxidative stress and promotes survival of *S. pneumoniae* during macrophage infections. In conclusion, NmlR was characterized as HOCl-sensing transcriptional regulator, which activates transcription of *adhC* under oxidative stress by thiol switches in *S. pneumoniae*.

KEYWORDS

H₂O₂, HOCl, NmlR, *Streptococcus pneumoniae*, thiol switches

1 | INTRODUCTION

The human pathogen *Streptococcus pneumoniae* (also called the pneumococcus) is a major cause of bacterial pneumonia and meningitis worldwide (CDC, 2020). During infections, *S. pneumoniae* is phagocytosed by immune cells, such as macrophages and neutrophils, which produce reactive oxygen species (ROS), such as superoxide anions and H₂O₂ as well as the highly reactive oxidant

hypochlorous acid (HOCl) within the respiratory burst to kill the invading pathogens (Gray et al., 2013; Ulfig & Leichert, 2021; Winterbourn et al., 2016; Winterbourn & Kettle, 2013). HOCl leads to oxidative damage of proteins, DNA and lipids (Gray et al., 2013; Ulfig & Leichert, 2021; Winterbourn et al., 2016). Among the many targets for oxidation by HOCl are the sulfur-containing amino acids cysteine and methionine in proteins. HOCl causes oxidative unfolding and aggregation of proteins, leading to

This is an open access article under the terms of the [Creative Commons Attribution-NonCommercial](https://creativecommons.org/licenses/by-nc/4.0/) License, which permits use, distribution and reproduction in any medium, provided the original work is properly cited and is not used for commercial purposes.

© 2022 The Authors. *Molecular Microbiology* published by John Wiley & Sons Ltd.

their loss of functions and bacterial killing (Ulfig & Leichert, 2021; Winter et al., 2008).

To cope with oxidative stress, *S. pneumoniae* utilizes the low molecular weight (LMW) thiol glutathione (GSH) as well as enzymatic ROS detoxification enzymes and thiol-disulfide oxidoreductases for the maintenance of the redox homeostasis (Mraheil et al., 2021; Yesilkaya et al., 2013). However, as facultative anaerobic bacterium, *S. pneumoniae* lacks the catalase and produces high amounts of endogenous H_2O_2 by the pyruvate oxidase SpxB and lactate oxidase LctO to promote bacterial colonization of the nasopharynx and to kill competing commensal and pathogenic bacteria in its niche (Mraheil et al., 2021; Pericone et al., 2003). Endogenously produced H_2O_2 has been shown to protect pneumococci against external H_2O_2 encountered during phagocytosis by host immune cells. For detoxification of oxygen, superoxide anion and H_2O_2 , the pneumococcus uses alternative antioxidant enzymes, such as the NADH oxidase (Nox), the superoxide dismutase (SodA), the thiol peroxidase (TpxD) and the alkyl hydroperoxidase (AhpD), which contribute to the oxidative stress resistance and virulence. In particular, the thiol peroxidase TpxD was H_2O_2 -inducible and conferred resistance towards external H_2O_2 stress (Mraheil et al., 2021; Yesilkaya et al., 2013). To repair oxidized Met residues under H_2O_2 stress at the bacterial surface, *S. pneumoniae* encodes the CTM electron transfer complex, composed the CcdA electron shuttle, extracellular thioredoxins (Etrx1/2) and the methionine sulfoxide reductase (MsrAB2), which are important for the virulence (Saleh et al., 2013). In addition, the ATP-dependent Clp protease, the DnaK/J-GrpE chaperones and the GroES/EL chaperonin machines are involved in the protein quality control and are assisted in their interaction with unfolded protein substrates by holdases and chaperedoxins, such as CnoX in *Escherichia coli*, to promote refolding of oxidatively damaged proteins (Dupuy & Collet, 2021; Mraheil et al., 2021; Ulfig & Leichert, 2021; Yesilkaya et al., 2013).

Furthermore, the pneumococcus encodes alternative transcriptional regulators, such as SpxR, Rgg, RitR, NmlR, CodY and SifR, which control enzymes involved in ROS generation and detoxification as well as other defense mechanisms required for bacterial survival during host-pathogen interactions (Mraheil et al., 2021; Yesilkaya et al., 2013; Zhang et al., 2022).

The MerR-family regulator NmlR has been characterized as transcriptional activator, which controls the expression of the *nmlR-adhC* operon under formaldehyde, methylglyoxal and S-nitrosoglutathione (GSNO) stress in *S. pneumoniae* (Potter et al., 2010; Stroehrer et al., 2007). The *adhC* gene encodes a class III alcohol dehydrogenase. These enzymes are widely distributed in prokaryotes and eukaryotes and function in detoxification of GSNO and S-hydroxymethylglutathione, the GSH adducts of nitric oxide (NO) and formaldehyde, respectively (Staab et al., 2008). While AdhC does not provide protection against carbonyl stress, it conferred resistance to GSNO stress in the pneumococcus, indicating that AdhC functions as GSNO reductase (Stroehrer et al., 2007). Furthermore, the $\Delta nmlR$ mutant was resistant to aerobic growth and produced lower endogenous H_2O_2 levels, which was caused by reduced transcription of the carbamoyl phosphate synthase-encoding *carB* gene (Potter et al., 2010).

These results established a link between NmlR and H_2O_2 resistance in the pneumococcus. Additionally, AdhC was required for systemic virulence of *S. pneumoniae* in a mouse model by promoting the survival in the blood (Stroehrer et al., 2007). Similarly, other MerR/NmlR homologs were characterized in *Haemophilus influenzae*, *Bacillus subtilis*, *Listeria monocytogenes*, *Neisseria gonorrhoeae* and *Neisseria meningitidis* and were shown to control the expression of conserved *adhC* genes, which conferred resistance under GSNO, H_2O_2 and carbonyl stress and during infections (Chen et al., 2013; Counago et al., 2016; Kidd et al., 2005; Nguyen et al., 2009; Supa-Amornkul et al., 2016).

However, the regulatory mechanisms of MerR/NmlR-family regulators still remain to be elucidated. MerR-family regulators often function as transcriptional activators, which bind to palindromic repeats in promoters with overlong spacers of 19–20bp between the –35 and –10 elements, which usually cannot be recognized by the RNA polymerase (RNAP) alone (Brown et al., 2003; Hobman et al., 2005; McEwan et al., 2011). Activation of the MerR-family transcription factor leads to conformational changes of the promoter, resulting in realignment of the promoter elements allowing recognition and initiation of transcription by the RNAP (Brown et al., 2003; Hobman et al., 2005; McEwan et al., 2011). In addition, MerR/NmlR-family regulators share a conserved Cys residue, which is required for redox-sensing of aldehyde and NO stress in *B. subtilis* AdhR and *N. gonorrhoeae* NmlR, respectively (Kidd et al., 2005; McEwan et al., 2011; Nguyen et al., 2009). While *B. subtilis* AdhR and *S. pneumoniae* NmlR are both single Cys-type redox-sensing regulators (Nguyen et al., 2009; Stroehrer et al., 2007), *N. gonorrhoeae* NmlR harbors four Cys residues, which function in Zn^{2+} coordination (Kidd et al., 2005). The activation mechanism of NmlR might involve post-translational thiol-modification of the conserved Cys by thiol-S-alkylation upon aldehyde exposure or by S-nitrosylation in response to NO stress (Chen et al., 2013; McEwan et al., 2011).

In this study, the NmlR regulon was identified as strongly upregulated under HOCl stress in the transcriptome of *S. pneumoniae* D39. Thus, we have further characterized the redox regulation of NmlR and the role of AdhC in the defense against HOCl and oxidative stress in *S. pneumoniae*. NmlR was oxidized by HOCl and ROS to form inter-subunit disulfides or S-glutathionylations in vitro, leading to activation of transcription initiation of *adhC* by the σ^{70} -RNAP holoenzyme in vitro, which required the conserved Cys52. AdhC was further important for protection of *S. pneumoniae* against ROS, HOCl and under macrophage infections, indicating that the NmlR regulon plays a crucial role under different host-derived redox stress conditions.

2 | RESULTS

2.1 | HOCl stress causes an oxidative and metal stress response and protein damage in the transcriptome of *S. pneumoniae* D39

To investigate the transcriptional response of *S. pneumoniae* D39 under HOCl stress, we analyzed the changes in the RNA-seq transcriptome after 30min of exposure to sub-lethal doses of 0.8mM

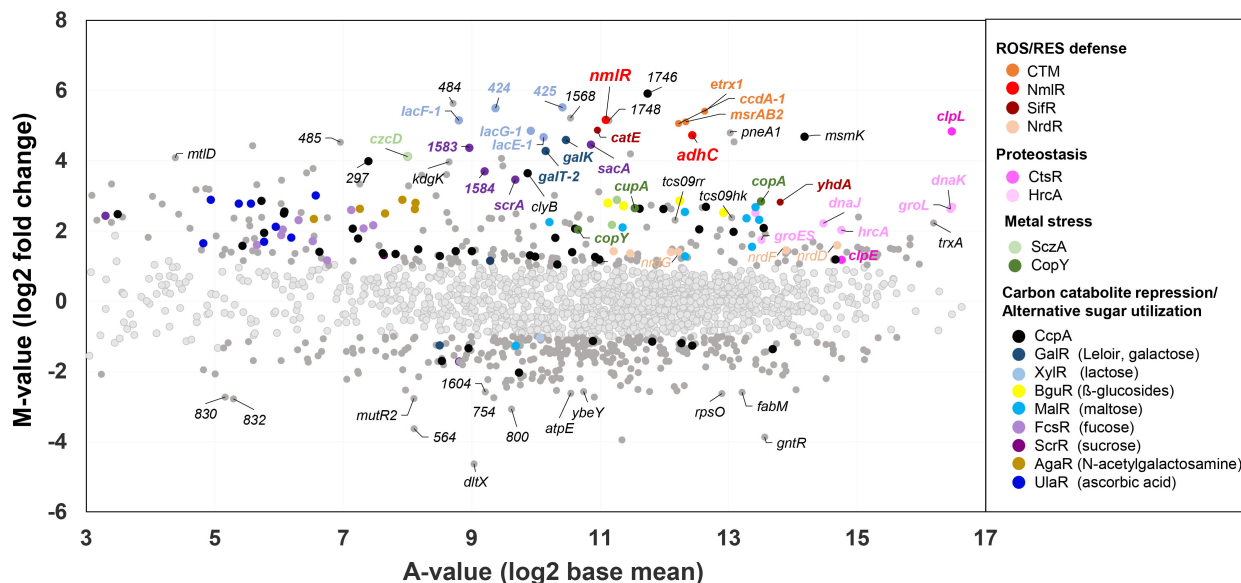


FIGURE 1 The RNA-seq transcriptome of *S. pneumoniae* D39 after HOCl stress. For RNA-seq transcriptomics, *S. pneumoniae* D39 was grown in supplemented RPMI medium to an OD_{600} of 0.4 and treated with 0.8 mM HOCl stress for 30 min. The gene expression profile of control versus HOCl stress is shown as ratio/intensity scatter plot (M/A-plot), which is based on the differential gene expression analysis using DeSeq2 as previously described (Love et al., 2014). Dark gray symbols indicate significantly induced and repressed transcripts upon HOCl stress (M -value ≥ 1 or ≤ -1 ; $p \leq 0.01$), while transcripts with light gray symbols are not significantly changed ($p > 0.01$). The most strongly upregulated regulons are color-coded and functionally classified into the ROS/RES defense (NmlR, SifR, NrdR, CTM operon), proteostasis (CtsR, HrcA), metal stress response (SczA, CopY) and carbon catabolite repression/alternative sugar utilization [GalR (Leloir, galactose), XylR (lactose), BguR (β -glucosides), MalR (maltose), FcsR (fucose), ScrR (sucrose), AgaR (N-acetylgalactosamine), UlaR (ascorbic acid)]. Among the downregulated regulons under HOCl stress are BlpR, CiaR, FabT, CodY, RitR, and RpoD, which are listed in Table S2. The complete transcriptome data and regulon classifications, including the up- and downregulated regulons are listed in Tables S1 and S2.

HOCl stress during the log phase of microaerophilic bacteria (Figure 1; Tables S1 and S2; Figure S1). For significant fold-changes (FC) of induced or repressed genes, the M -value cutoff (\log_2 FC HOCl vs. control) of $m \geq 1.0$ and $m \leq -1.0$ was chosen (adjusted p -value ≤ 0.01). Accordingly, 296 and 306 genes were significantly ≥ 2 -fold up- and downregulated, respectively, in *S. pneumoniae* D39 under HOCl stress. These HOCl-responsive genes were classified into known regulons and visualized by color codes in the M/A ratio intensity scatter plot (Figure 1; Tables S1 and S2).

First, we were interested to reveal the redox-controlled regulons, which contribute to the defense against oxidative and electrophile stress and respond most strongly to HOCl stress in the pneumococcus. Among the top-scorers was the CTM electron complex, encoded by the *ccdA1-etrxA1-msrAB2* operon (33.4–42.5-fold), which is involved in the oxidative stress response and functions in reduction of oxidized methionine residues of cell envelope proteins in *S. pneumoniae* (Gennaris & Collet, 2013; Saleh et al., 2013). In addition, the *trxA* and *trxB* genes (4.7- and 3.8-fold) encoding the cytoplasmic thioredoxin (Trx)/thioredoxin reductase system, were upregulated by HOCl stress, indicating an increased protein thiol-oxidation in *S. pneumoniae*. Interestingly, the *nmlR* (36-fold) and *adhC* (26.5-fold) genes were among the most strongly HOCl-induced transcripts in the pneumococcal transcriptome (Figure 1; Tables S1 and S2). This suggests an important role of AdhC in the HOCl stress defense, which was investigated in more

detail (see next sections). Furthermore, HOCl stress caused the strong induction of the quinone-responsive SifR regulon, including the *catE* (29.2-fold) and *yhdA* (7.1-fold) genes, which encode the catechol-2,3-dioxygenase and NAD(P)H-dependent FMN ferric reductase, respectively (Zhang et al., 2022). In addition, transcription of NrdR-controlled *SPD_0187-0191* operon, encoding the anaerobic ribonucleoside triphosphate reductase, was weakly (2.6–3-fold) upregulated by HOCl stress (Figure 1; Tables S1 and S2). The NrdR homolog of *Mycobacterium smegmatis* has been previously identified as reversibly oxidized in its Zn^{2+} ribbon motif (Hillion et al., 2017), suggesting that the repressor could be also inactivated by HOCl in *S. pneumoniae*.

Due to increased protein thiol-oxidation and aggregation, the CtsR-controlled Clp proteases, such as *clpL* (28.6-fold) and *clpE* (2.3-fold), and the HrcA-regulated chaperones encoded by the *hrcA-grpE-dnaK-dnaJ* (3.4–6.2-fold) and *groL-groES* (4.1–6.5-fold) operons were highly upregulated under HOCl stress in the *S. pneumoniae* transcriptome (Figure 1; Tables S1 and S2). This protein quality control machinery of proteases and chaperones is required for protein folding and degradation of oxidatively damaged proteins under HOCl stress (Mraheil et al., 2021; Yesilkaya et al., 2013).

Among the top hits was further the Zn^{2+} efflux pump-encoding *czcD* gene (17.4-fold), which is transcribed upstream of the *nmlR-adhC* operon and controlled by the TetR-family regulator SczA (Kloosterman et al., 2007). HOCl also caused the induction of the

copper-controlled CopY regulon (4.1–7.2-fold), including *cupA* and the copper-transport ATPase-encoding *copA* gene (Shafeeq et al., 2011). In addition, the RegR regulon required for virulence, adherence and competence of *S. pneumoniae*, was strongly induced by HOCl stress (2.1–15.7-fold) (Chapuy-Regaud et al., 2003) (Tables S1 and S2). As another virulence factor, the pneumococcal adherence and virulence factor B *pavB* was strongly (23.3-fold) induced by HOCl stress.

Interestingly, HOCl stress also caused the induction of several regulons involved in the uptake and utilization of alternative carbohydrates, which serve as energy and carbon sources in the absence of glucose and are important for virulence in *S. pneumoniae* (Minhas et al., 2021). The induction of these sugar catabolic regulons was accompanied by the derepression of 76 genes of the CcpA regulon (2–50.5-fold), indicating that CcpA is partially inactivated after HOCl exposure in the pneumococcus (Figure 1; Tables S1 and S2). The most strongly induced disaccharide utilization systems were the XylR (25.5–45.9-fold) and ScrR regulons (5.4–22-fold), which include the ABC and PTS transporters and catabolic enzymes for the hydrolysis of lactose and sucrose, respectively (Minhas et al., 2021). Among the HOCl-induced regulons were further GalR (19.4–24.1-fold) and LacR (4.5–7.4-fold), comprising the enzymes of the Leloir and tagatose 6-phosphate pathways for catabolism of galactose and lactose (Minhas et al., 2021). Furthermore, the BguR, FcsR, RafR, MalR, AgaR and UlaR regulons required for the acquisition and catabolism of β -glucosides, fucose, raffinose, maltose, *N*-acetylgalactosamine and ascorbic acid, respectively (Minhas et al., 2021), were upregulated at lower levels (2.2–8.1-fold) upon HOCl stress. Taken together, the upregulation of many utilization systems for alternative carbohydrates suggests that HOCl stress might affect either directly or indirectly the regulation of carbon catabolite repression.

In other bacteria, HOCl stress was shown to cause strong ATP depletion, which correlated with the loss of viability (Barrette et al., 1989; Ulfig & Leichert, 2021). Since HOCl exposure affected also the growth in the pneumococcus (Figure S1H), the ATP synthase subunits-encoding genes (*atpF* and *atpE*) and genes for ribosomal proteins were downregulated in the HOCl stress transcriptome (Figure 1, Table S1 and S2). Furthermore, the *fabT*, *fabM*, *fabH* and *acpP* genes required for fatty acid biosynthesis showed decreased transcription (2.3–6-fold) in HOCl-treated cells.

2.2 | The NmlR regulon responds most strongly to methylglyoxal, formaldehyde and HOCl stress in *S. pneumoniae*

Due to its strong induction under HOCl stress, the NmlR regulon was selected to study in more detail the redox-sensing mechanism of NmlR and the role of AdhC under oxidative stress in the pneumococcus. The *nmlR-adhC* operon was previously shown to respond strongly to formaldehyde, methylglyoxal and GSNO stress in *S. pneumoniae* (Potter et al., 2010; Stroehrer et al., 2007). qRT-PCR analysis was used to monitor the expression profile of *adhC* in *S. pneumoniae* D39 after exposure to sub-lethal doses of

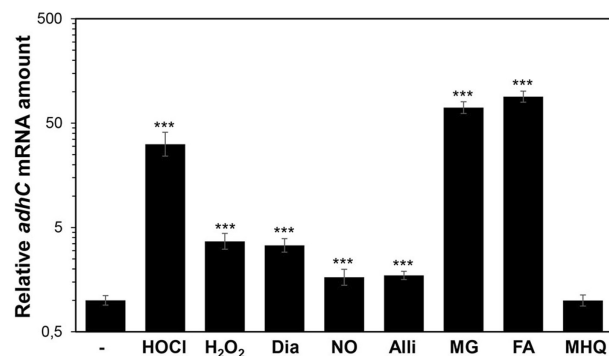


FIGURE 2 Transcription of *adhC* is most strongly induced after aldehyde and HOCl stress in *S. pneumoniae* D39. For qRT-PCR analysis, *S. pneumoniae* D39 was grown in supplemented RPMI medium to an OD₆₀₀ of 0.4 and exposed to different thiol-reactive compounds for 30 min, including 0.8 mM HOCl, 0.45 mM H₂O₂, 4 mM diamide, 0.167 mM DEA-NONOate as NO donor (NO), 0.4 mM alliin (Alli), 0.325 mM methylglyoxal (MG), 0.3 mM formaldehyde (FA) and 10 mM methylhydroquinone (MHQ). Transcription of *adhC* was analyzed by qRT-PCR before (–) and after stress exposure. The stress-induced *adhC* transcript levels were normalized to the *adhC* mRNA level of untreated cells, which was set to a fold-change of 1. Error bars represent the standard deviation of 3 biological replicates with 2 technical replicates each. Statistical differences to the control were determined using one-way ANOVA and Dunnett's multiple comparisons test. * $p \leq 0.05$; ** $p \leq 0.01$ and *** $p \leq 0.001$.

different thiol-reactive compounds, such as 0.8 mM HOCl, 0.45 mM H₂O₂, 4 mM diamide, 0.167 mM diethylamine (DEA)-NONOate, 0.4 mM alliin, 0.325 mM methylglyoxal, 0.3 mM formaldehyde and 10 mM methylhydroquinone (MHQ) (Figure 2; Figure S1). The qRT-PCR results confirmed the strongest induction of the *nmlR-adhC* operon under aldehyde stress (70.4–89.6-fold) (Potter et al., 2010). Consistent with the transcriptome data, *adhC* transcription was strongly increased after HOCl treatment (31.4-fold). Exposure to the NO donor, alliin, H₂O₂ and diamide resulted in a much weaker induction of *adhC* (1.7–3.7-fold). In addition, *adhC* transcription was not upregulated by MHQ. These results indicate that the NmlR regulon responds most strongly to reactive aldehydes and the strong oxidant HOCl in *S. pneumoniae* D39.

2.3 | The conserved Cys52 of NmlR is essential for redox-sensing of HOCl stress in vivo

To study the function of the conserved Cys52 of NmlR for redox sensing of HOCl stress, we analyzed transcriptional activation of *adhC* in the Δ *nmlR* mutant and in the *nmlR*- and *nmlR*C52A-complemented strains under control and HOCl stress conditions by qRT-PCR (Figure 3a). While *adhC* transcription was strongly (17.6-fold) upregulated in the wild type (WT) under HOCl stress, the transcript level of *adhC* was decreased in the Δ *nmlR* mutant under HOCl stress. These results support that NmlR acts as transcriptional activator of the *nmlR-adhC* operon under HOCl stress. In agreement with previous

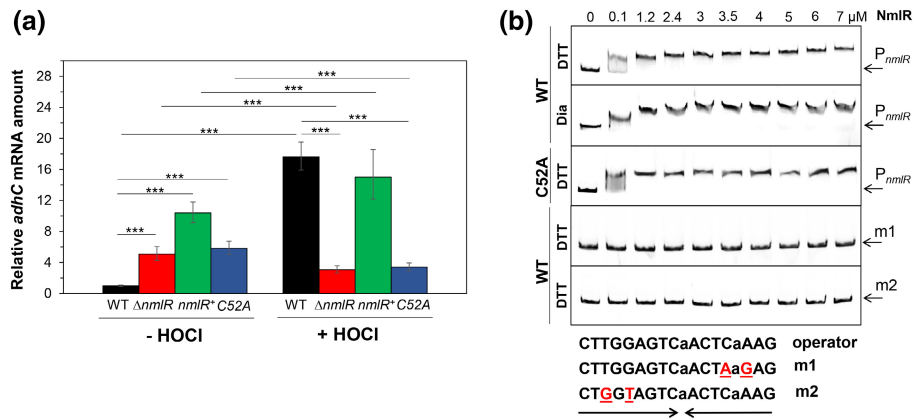


FIGURE 3 NmlR activates *adhC* transcription under HOCl stress in vivo (a) and binds to the *nmlR*-*adhC* promoter in vitro (b). (a) Transcription of *adhC* was analyzed using qRT-PCR in the *S. pneumoniae* D39 WT, the $\Delta nmlR$ mutant as well as the *nmlR*⁺ and *nmlR*C52A complemented strains, which were grown in RPMI to an OD_{600} of 0.4 and harvested before (-HOCl) and 30 min after exposure to 0.8 mM HOCl stress (+HOCl). The HOCl-induced *adhC* transcript levels in the mutant and complemented strains were normalized to the mRNA level of *adhC* in the WT without HOCl, which was set to a fold-change of 1. Error bars represent the standard deviation of 3 biological replicates with 2–4 technical replicates each. The statistics was determined using one-way ANOVA and Dunnett's multiple comparisons test. ** $p \leq 0.01$ and *** $p \leq 0.001$. (b) NmlR binds to the palindromic sequence upstream of the *nmlR*-*adhC* operon under reducing and oxidizing conditions. EMSAs were used to analyze the DNA-binding activity of increasing amounts (0.1–7 μ M) of NmlR and NmlRC52A to 15 ng of the *nmlR* promoter (P_{nmlR}) in vitro. To analyze the specific binding to the palindrome, two base substitutions were introduced in each half of the inverted repeat, denoted in red (m1 and m2). The arrows denote the free DNA probe and the shifted band indicates the DNA-NmlR promoter complex. The EMSA experiments were performed in 3 replicates.

studies (Potter et al., 2010), *adhC* transcription was 5.1-fold enhanced in the untreated $\Delta nmlR$ mutant, suggesting that NmlR might repress *adhC* transcription under control conditions. In contrast, decreased *adhC* levels were found in the untreated $\Delta nmlR$ mutant in another study (Stroeher et al., 2007). Surprisingly, *adhC* transcription was further increased under control conditions in the pBAV-*nmlR*-complemented strain, in which *nmlR* is constitutively expressed under the erythromycin cassette promoter pE of plasmid pBAV1CpE (Hess et al., 2017), suggesting that constitutive overproduction of NmlR might also lead to activation of *adhC* transcription (Figure 3a). Upon HOCl stress, the expression level of *adhC* was further elevated in the *nmlR*-complemented strain, supporting that NmlR activates *adhC* transcription upon HOCl exposure. In contrast, the transcriptional level of *adhC* was low in the HOCl-treated *nmlR*C52A mutant, indicating that Cys52 is required for redox-sensing and transcriptional activation by NmlR. These results revealed that NmlR acts as redox-sensing activator of *adhC* transcription under HOCl stress, depending on the conserved Cys52 in vivo.

2.4 | NmlR binds specifically to the *nmlR*-*adhC* operator in the reduced and oxidized state

NmlR was proposed to bind to the 9–9 bp palindromic operator sequence CTTGGAGTC-aACTCaAAG, located between the –35 and –10 promoter elements (Stroeher et al., 2007). However, experimental evidence for the specific binding of NmlR to the operator is still missing. Thus, gel electrophoretic mobility shift assays (EMSAs) were used to investigate the DNA-binding activity of

purified NmlR protein to the *nmlR*-*adhC* operon promoter in vitro. The gel-shift results showed that purified reduced NmlR protein binds to the *nmlR* promoter probe, which is indicated by the band shift in the NmlR-DNA-binding reactions (Figure 3b). To analyze the specific binding of NmlR to the predicted operator sequence, we exchanged two nucleotides in each half of the inverted repeat (m1: C to A and A to G; m2: T to G and G to T) and analyzed the DNA-binding activity of NmlR to these mutated promoter probes (Figure 3b). NmlR was unable to bind to the mutated palindromic sequences m1 and m2 in vitro, supporting the specific binding of NmlR to the 9–9 bp palindromic sequence.

Next, the effect of thiol-oxidation on the DNA-binding activity of NmlR was assessed using the EMSAs. Treatment of NmlR with increasing concentrations of diamide did not affect the DNA-binding activity (Figure 3b). Similarly, the DNA-binding activity was not impaired under HOCl stress (data not shown). These results are in accordance with previous data, demonstrating that MerR-family regulators interact with their cognate DNA both in the presence and absence of the specific inducers (Brown et al., 2003; Fang & Zhang, 2022). In response to specific signals, MerR proteins undergo a conformational change, leading to a DNA distortion and reorientation of the –35 and –10 elements for RNAP recognition (Brown et al., 2003; Fang & Zhang, 2022).

Since the single Cys52 of NmlR was identified as essential for activation of *adhC* transcription upon HOCl stress, we analyzed the role of Cys52 for the DNA-binding activity of NmlR in gel shift assays. The reduced NmlRC52A mutant protein showed a similar DNA-binding affinity compared to NmlR (Figure 3b), indicating that Cys52 is not required for the DNA-binding activity of NmlR.

2.5 | NmlR is oxidized to intermolecular disulfides or S-glutathionylated at the redox-sensing Cys52 in vitro

To investigate the redox-sensing mechanism, the post-translational thiol modifications of NmlR were analyzed in response to different oxidants, such as diamide, H₂O₂ and HOCl. Using non-reducing SDS-PAGE, NmlR was shown to be completely oxidized to form intersubunit disulfides after treatment with the oxidants (Figure 4a–c). As expected, the intermolecular disulfides could be reversed in the reducing SDS-PAGE analysis (Figure 4a–c). Since NmlR represents a one-Cys-type redox-sensing regulator, it could also sense HOCl and H₂O₂ stress by formation of mixed disulfides at Cys52 with the LMW thiol GSH, termed as S-glutathionylation. As shown in Figure 4c, the treatment of NmlR with 1–2 mM H₂O₂ in the presence of GSH led only to partial formation of the disulfide-linked dimers, indicating that GSH prevented the complete intermolecular disulfide formation.

Matrix-assisted laser desorption ionization-time of flight-mass spectrometry (MALDI-TOF-MS) was used to identify the post-translational thiol-modifications of reduced and oxidized NmlR after digestion with trypsin. In the MS1 scan of the peptides of the reduced NmlR sample, a peptide was identified with the *m/z* of 482.19 Da, corresponding to the carbamidomethylated CFR peptide (Figure 5a). In the H₂O₂-oxidized samples of the disulfide-linked dimer without or with GSH, this CFR-CAM peptide was absent and instead a peptide with the *m/z* of 847.43 Da was detected, confirming the oxidation of NmlR to the Cys52-Cys52' intermolecular disulfide (Figure 5b,c). In addition, the S-glutathionylated CFR peptide was detected as peak at *m/z* of 730.30 Da in the lower gel band

of the oxidized NmlR sample, which was treated with H₂O₂ in the presence of GSH (Figure 5d). In conclusion, our data support that NmlR functions as redox-sensing transcriptional activator of the *nmlR-adhC* operon that senses oxidants by reversible thiol switches, including intersubunit disulfides or S-glutathionylations in vitro.

2.6 | NmlR activates transcription at the *nmlR* promoter in the oxidized intersubunit disulfide and S-glutathionylated form by the *Escherichia coli* σ^{70} -RNAP in vitro, depending on the conserved Cys52

To test the activation of transcription initiation by NmlR at the *nmlR-adhC* operon promoter, in vitro transcription by *E. coli* σ^{70} -RNAP was monitored from a plasmid that harbors the broccoli fluorescent light-up RNA aptamer (broccoli-FLAP) as fluorescent reporter (Filonov et al., 2014; Huang et al., 2022), downstream of the *nmlR* promoter (Figure 6). Upon transcription, the broccoli aptamer adopts a defined three-dimensional fold that provides the binding platform for the fluorogen DFHBI-1T (Filonov et al., 2014; Huang et al., 2022). By binding to broccoli-FLAP, DFHBI-1T emits fluorescence (emission = 507 nm), which serves as a readout for transcription. An initial lag phase (*t*₀) determines the time in which a first complete broccoli-FLAP is transcribed, folded and bound by DFHBI-1T. The lag phase is followed by a linear increase in fluorescence and the slope corresponds to the initial transcription rate or relative transcription initiation rate, respectively. Multi-round transcription showed that broccoli-FLAP production by RNAP in the presence of TCEP-reduced NmlR (NmlR_{red}) and NmlR52A (C52A_{red}) proteins significantly

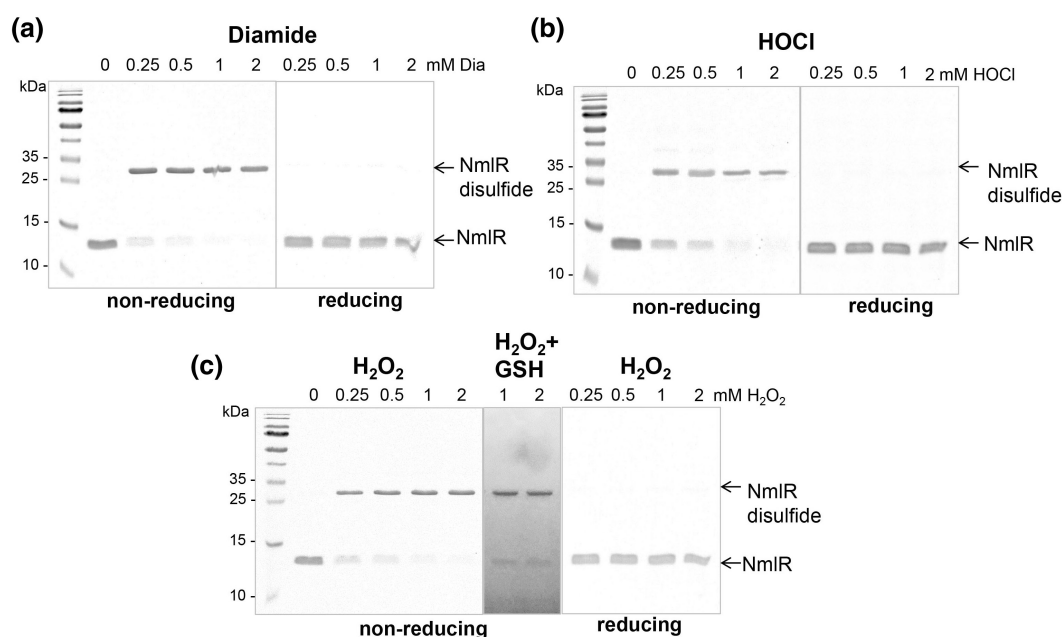


FIGURE 4 NmlR is oxidized to intermolecular disulfides upon treatment with the oxidants diamide, HOCl and H₂O₂ in vitro. (a–c) The purified NmlR protein was treated with increasing amounts (0.25–2 mM) of diamide (a), HOCl (b) and H₂O₂ (c) for 15 min in vitro and subjected to non-reducing SDS-PAGE analysis. (c) NmlR was oxidized either with H₂O₂ alone or with 1 and 2 mM H₂O₂ in the presence of 0.1 and 0.2 mM GSH. The reduction of the NmlR disulfides is shown in the reducing SDS-PAGE analyses.

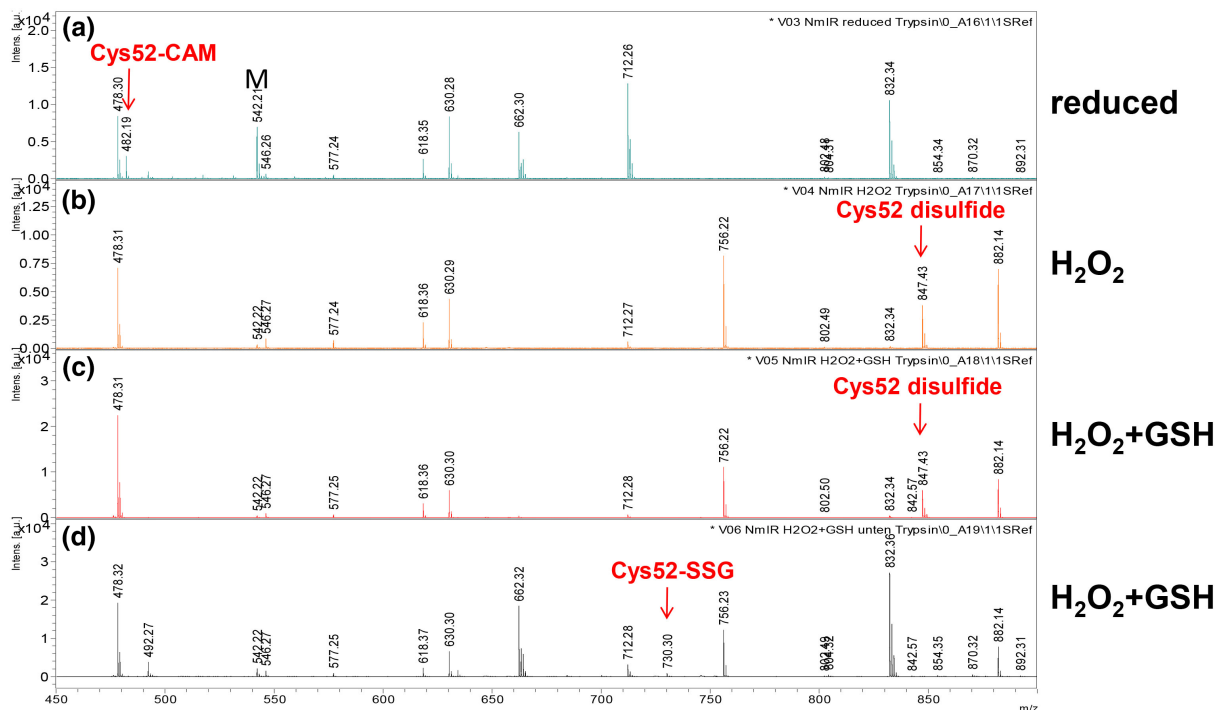


FIGURE 5 NmlR can be oxidized by H_2O_2 to intermolecular disulfides and *S*-glutathionylated in the presence of GSH in vitro as revealed by MALDI-TOF MS. The bands of the reduced NmlR and the oxidized NmlR intermolecular disulfide-linked dimer were digested with trypsin and the peptides analyzed by MALDI-TOF MS. The MS1 spectra are displayed in the m/z range of 450–900 showing the mass peaks of the small C_{52} FR peptide in the (a) reduced and (b–d) H_2O_2 -oxidized NmlR samples without or with GSH. (a) Cys52 is fully carbamidomethylated (m/z 482.19 Da) in reduced NmlR. (b) Treatment of NmlR with H_2O_2 alone leads to oxidation to the C52–C52' intersubunit disulfide peptide (m/z 847.43 Da). (c) Oxidation with H_2O_2 in the presence of GSH leads to the formation of the C52–C52' intersubunit disulfide-linked dimer and (d) the *S*-glutathionylated Cys52 peptide (m/z 730.30 Da) as labeled in the non-reducing SDS-PAGE analysis in Figure 4.

decreases the relative initiation rate to 0.39 and 0.53, respectively, compared to 1 by RNAP alone (Figure 6). This indicates that reduced NmlR represses transcription initiation by *E. coli* RNAP at the *nmlR* promoter, which does not depend on C52A. In contrast, relative initiation rates are significantly increased to 3.9 and 2.2 through oxidation of NmlR to the intersubunit disulfide (NmlR_{ox}) by H_2O_2 alone or to the *S*-glutathionylated form (NmlR_{GSH}) by H_2O_2 in the presence of GSH, respectively. However, transcription initiation rates by RNAP were not significantly changed with both H_2O_2 -treated C52A proteins (C52A_{ox} and C52A_{GSH}), supporting that the conserved Cys is important for transcriptional activation via its thiol-switches. These data support the model that NmlR is activated by different thiol-switches, such as intersubunit disulfides and *S*-glutathionylations, leading to enhanced transcription of the *nmlR*-*adhC* operon by the RNAP, while reduced NmlR represses transcription.

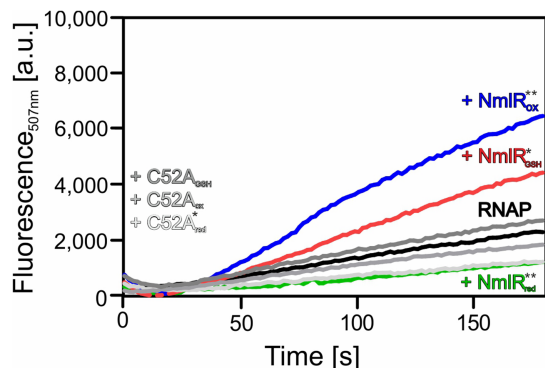
2.7 | The alcohol dehydrogenase AdhC functions in the defense against HOCl and H_2O_2 stress in *S. pneumoniae* D39

To investigate the role of AdhC in the protection against oxidative stress in *S. pneumoniae*, growth and survival analyses of the $\Delta nmlR$ and $\Delta adhC$ mutants were performed under HOCl and H_2O_2 stress

(Figure 7). The growth of both mutants was significantly impaired after treatment with sub-lethal doses of 0.8 mM HOCl as compared to the WT (Figure 7a,c). In addition, the $\Delta nmlR$ and $\Delta adhC$ mutants displayed 13.4%–17% decreased survival rates after 3 h and 4 h exposure to the lethal dose of 1.1 mM HOCl (Figure 7e). While the growth of the $\Delta nmlR$ mutant was not affected by sub-lethal H_2O_2 stress, treatment with lethal 1 mM H_2O_2 resulted in decreased survival rates of the $\Delta nmlR$ mutant compared to the WT (Figure 7d,f). Similarly, the $\Delta adhC$ mutant showed a higher sensitivity towards lethal H_2O_2 stress, indicated by the 1.7–2.3-fold lower survival rates than the WT. The growth and survival defects of both mutants could be restored back to the WT level in the *nmlR* and *adhC*-complemented strains, respectively (Figure 7e,f and Figure S2). In contrast, the *nmlR*C52A mutation was unable to complement the HOCl- and H_2O_2 -sensitive phenotypes of the $\Delta nmlR$ mutant (Figure 7b,e,f). These results indicate that Cys52 is important for activation of *adhC* expression and that AdhC confers resistance towards HOCl and ROS stress in *S. pneumoniae* D39.

2.8 | The NmlR regulon confers protection against the oxidative burst of human macrophages

To analyze the role of the NmlR regulon in the defense of macrophage-derived ROS production under infection conditions,



| Sample | t_0 [s] | Initial rate [s ⁻¹] | Relative initiation rate |
|-----------------------|-----------|---------------------------------|--------------------------|
| RNAP | 15.7 | 13.5 ± 0.3 | 1.00 ± 0.02 |
| + NmlR _{ox} | 19.9 | 52.4 ± 6.8 | 3.88 ± 0.50 |
| + NmlR _{red} | 24.3 | 5.3 ± 1.9 | 0.39 ± 0.14 |
| + NmlR _{GSH} | 17.4 | 30.0 ± 3.3 | 2.22 ± 0.24 |
| + C52A _{ox} | 31.1 | 11.1 ± 1.3 | 0.82 ± 0.10 |
| + C52A _{red} | 10.6 | 7.2 ± 1.4 | 0.53 ± 0.10 |
| + C52A _{GSH} | 15.7 | 16.3 ± 2.3 | 1.21 ± 0.17 |

FIGURE 6 The NmlR intersubunit disulfide and S-glutathionylated NmlR activate *adhC* transcription by *E. coli* σ^{70} -RNAP in vitro, which depends on the single Cys52. To compare transcriptional initiation efficiencies at the *nmIR-adhC* operon promoter by the *E. coli* σ^{70} -RNAP and reduced, oxidized and S-glutathionylated NmlR (NmlR_{red}, NmlR_{ox} and NmlR_{GSH}) and NmlRC52A mutant proteins (C52A_{red}, C52A_{ox} and C52A_{GSH}), the broccoli-FLAP assay was used (see experimental Procedures). Transcription of complete broccoli-FLAP is reported by binding of a pro-fluorophore to the aptamer, leading to an increase in fluorescence emission at 507 nm. The initial slopes in the curves represent the relative initiation rates of transcription. The table shows the calculated values of linear fits of the initial increases in fluorescence as determined after time offset t_0 for the reaction of RNAP without or with NmlR or C52A proteins, which were oxidized with 2.5% H₂O₂ in the absence (NmlR_{ox}, C52A_{ox}) or presence of 0.3 mM GSH (NmlR_{GSH}, C52A_{GSH}) or reduced with 10 mM TCEP (NmlR_{red}). Data represent means ± SD of three independent experiments, using the same biochemical samples. Significance was assessed using an unpaired, two-sided *t*-test. **p* < 0.05; ***p* < 0.01.

we determined the intracellular survival of the $\Delta nmIR$ mutant in the human macrophage cell line THP-1A (Figure 8a). The colony-forming units (CFUs) of intracellular *S. pneumoniae* were determined 2 to 5 h post-infection (p.i.) (Figure 8a). The results revealed that the $\Delta nmIR$ mutant was significantly impaired in survival inside human macrophages. Specifically, at 3 h p.i., the number of viable bacteria decreased to 53.9% for the WT and to 26.7% for the $\Delta nmIR$ mutant (Figure 8a). Thus, the $\Delta nmIR$ mutant showed a 50% reduced survival rate compared with the WT after 3 h p.i. This sensitivity of the $\Delta nmIR$ mutant could be abolished by the addition of the flavoprotein inhibitor diphenyleneiodonium (DPI) (Figure 8a). DPI was previously

shown to inhibit NOX2 and the macrophage NO synthase to prevent ROS and NO generation (Altenhofer et al., 2015; O'Donnell et al., 1993; Stuehr et al., 1991). Thus, DPI treatment increased the survival rate of both *S. pneumoniae* strains to >90% after 3 h p.i. (Figure 8a). Interestingly, the protective effect of DPI was less pronounced after 4 and 5 h p.i., probably indicating the onset of other killing mechanisms. Nevertheless, also at these later time points, the survival of the $\Delta nmIR$ mutant was significantly improved through inhibition of the oxidative burst. Under control conditions, the $\Delta nmIR$ mutant showed a 2.4–2.5-fold lower survival than the WT, whereas the viability rate was only 1.5–1.8-fold decreased after DPI addition.

Since DPI was shown to affect the phagocytosis rate (Lv et al., 2017; Zhu et al., 2017), phagocytosis assays were performed to exclude differences in the internalization of the WT and the $\Delta nmIR$ mutant. DPI significantly decreased the phagocytosis rate of THP-1A cells ~16.5-fold (Figure 8b). However, the phagocytosis rate of both strains by THP-1A cells was comparable in the absence and presence of DPI (Figure 8b). These results indicate that the NmlR-controlled AdhC is important for the defense against oxidative stress and contributes to the resistance of *S. pneumoniae* D39 against the respiratory burst during macrophage infections.

3 | DISCUSSION

In this work, we have used RNA-seq transcriptome analysis to study the expression profile of *S. pneumoniae* in response to the strong oxidant HOCl. The transcriptome signature revealed that HOCl stress caused the most prominent induction of the thiol-specific oxidative stress response, indicated by the extracellular CTM complex for repair of oxidized Met residues (Gennaris & Collet, 2013; Saleh et al., 2013), the NmlR-controlled *adhC* gene (Potter et al., 2010; Stroehrer et al., 2007) and the CtsR and HrcA regulons for repair or degradation of oxidatively damaged proteins (Mraheil et al., 2021; Yesilkaya et al., 2013). In addition, the quinone-responsive SifR regulon (Zhang et al., 2022) and the CopY and SczA regulons controlling metal efflux systems (Kloosterman et al., 2007; Shafeeq et al., 2011) were strongly induced by HOCl stress. The upregulation of these metal efflux systems might be related to the HOCl-induced oxidation of metal-coordinating Cys residues of metal regulators (Fliss & Menard, 1991), accounting perhaps for the pneumococcal SczA and CopY regulators and the related ArsR and CopR repressors of *B. subtilis* (Chi et al., 2011). Similarly, the NrdR repressor of *M. smegmatis* harbors Zn²⁺-coordinating Cys residues, which were previously found oxidized by HOCl stress in the redox proteome, leading to derepression of the NrdR regulon in the transcriptome (Hillion et al., 2017). Thiol-oxidation of NrdR by HOCl stress therefore most likely explains the weak upregulation of the NrdR regulon in the transcriptome of *S. pneumoniae*.

However, the single Cys residue of the activator SczA was not required for metal binding, which involves rather His and Glu residues (Martin et al., 2017), suggesting other mechanisms accounting for the induction of the zinc efflux systems by thiol-reactive compounds.

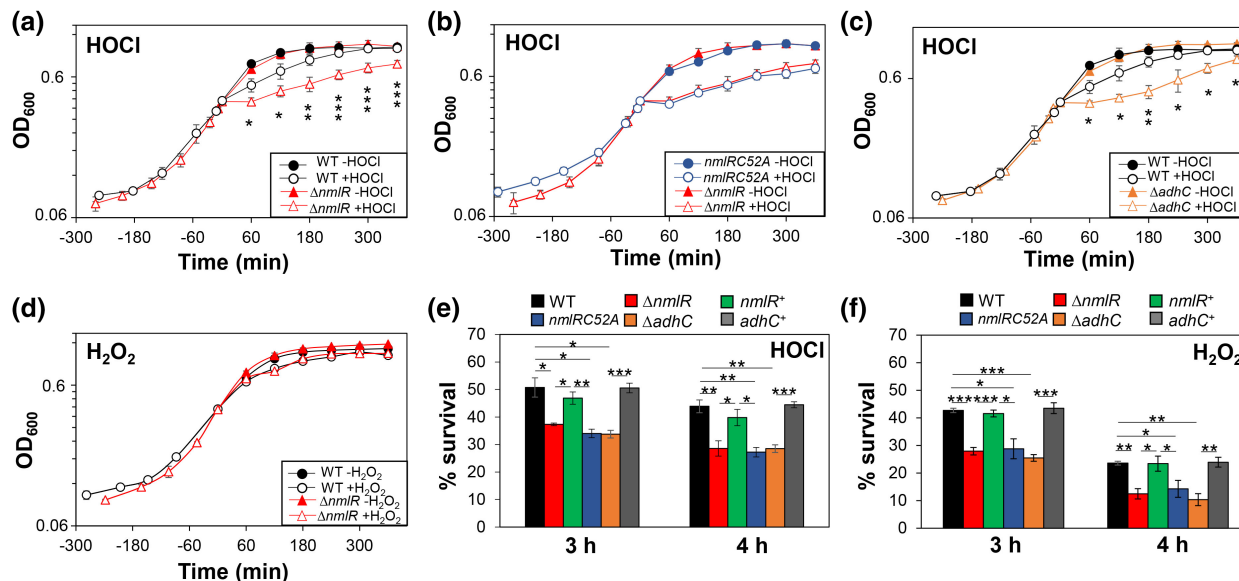


FIGURE 7 The Nmr regulon confers resistance to HOCl and H₂O₂. Growth curves (a–d) and survival assays (e and f) were performed with *S. pneumoniae* D39 WT, the $\Delta nmIR$ and $\Delta adhC$ mutants as well as the $nmIR^+$, $nmIRC52A$ and $adhC^+$ complemented strains in RPMI medium. At an OD₆₀₀ of 0.4, bacteria were treated with sub-lethal doses of 0.8 mM HOCl and 0.45 mM H₂O₂ for growth phenotypes and survival data, which were acquired 3 and 4 h after exposure to 1.1 mM HOCl and 1 mM H₂O₂. The survival rates of CFUs for the treated samples were calculated relative to the untreated control, which was set to 100%. Growth curves of the $nmIR^+$ - and $adhC^+$ -complemented strains are shown in Figure S2. The results are from 3–5 biological replicates. Error bars represent the standard deviation. The statistics was calculated using a Student's unpaired two-tailed t-test. * $p < 0.05$; ** $p < 0.01$; *** $p < 0.001$.

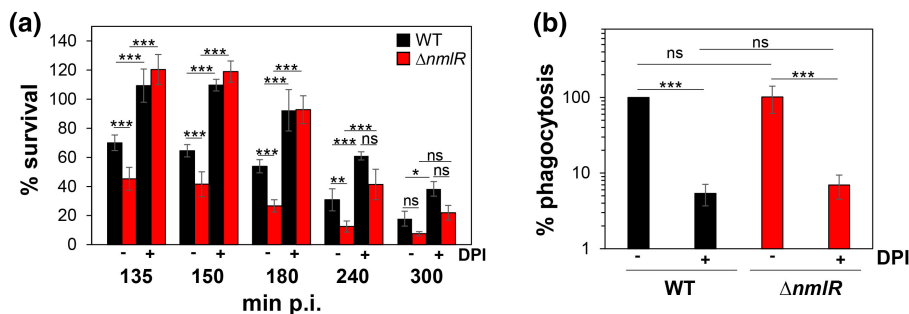


FIGURE 8 The $\Delta nmIR$ mutant is impaired in survival inside THP-1A human macrophages. (a) The survival of *S. pneumoniae* D39 WT and the $\Delta nmIR$ mutant was analyzed without or with diphenyleneiodonium chloride (DPI) at 135, 150, 180, 240 and 300 min post-infection (p.i.) of the human macrophage cell line THP-1A. The percentage of survival was calculated for the time points above by normalizing them to the 2 h time point, which was set to 100%. (b) The relative phagocytosis rate was determined for *S. pneumoniae* D39 WT and the $\Delta nmIR$ mutant by analyzing the CFUs 2 h after infection relative to the input values and displayed in relation to the WT without DPI treatment, which was set to 100%. The results are from four biological replicates and the error bars represent the standard deviation. The statistics was calculated using one-way ANOVA and Dunnett's multiple comparisons test. $^{ns}p > 0.05$; * $p < 0.05$; ** $p < 0.01$; *** $p < 0.001$.

Previous studies established that the LMW thiol bacillithiol (BSH) of *B. subtilis* functions as efficient metal buffer, forming an intracellular BSH₂Zn²⁺ pool, which is even more sensitive to thiol-oxidation than protein-bound Zn²⁺, leading to Zn²⁺ release and BSH oxidation to bacillithiol disulfides (BSSB) (Ma et al., 2014). This Zn²⁺ release from BSH stores resulted in induction of the *czcD* and *cadA* genes through inactivation of the CzcR repressor in *B. subtilis*. This further explained the induction of the CzcR regulon by many thiophilic metal ions and by reactive carbonyl electrophiles, which rapidly deplete the BSH pool (Chandrangsu et al., 2014; Moore et al., 2005; Nguyen et al., 2009). Consequently, the increased Zn²⁺ level released from

related GSH₂Zn²⁺ stores due to GSH oxidation might activate SczA to trigger induction of the Zn²⁺ efflux system CzcD in the pneumococcus, which remains to be investigated in more detail in future studies.

Overall, similar thiol-specific oxidative, electrophile and metal stress responses were previously reported under HOCl stress in other Gram-positive bacteria, such as *Staphylococcus aureus* and *B. subtilis* (Chi et al., 2011; Loi et al., 2018). Due to its high reactivity with thiols (Storkey et al., 2014), HOCl generally induced most known regulons controlled by redox-sensing regulators in the different bacteria. The prominent induction of the HrcA- and

CtsR-controlled proteases and chaperones under HOCl stress is conserved throughout firmicutes, supporting that HOCl causes increased protein thiol-oxidation and protein aggregation. However, since the bacteria had to be cultivated in the supplemented RPMI cell culture medium for optimal growth and to avoid starvation conditions, HOCl could also react with primary amines of medium components, leading to formation of less-reactive chloramines (Ashby et al., 2020; Peskin & Winterbourn, 2001). Thus, the question arises whether the HOCl-induced transcriptome changes in *S. pneumoniae* are due to HOCl or the chloramines as reaction product of HOCl. In general, the chosen concentration of 0.8 mM HOCl was sub-lethal and caused a half-maximal growth rate in agreement with standard conditions of physiological stress experiments. Consequently, the transcriptome profiles of the general thiol-specific oxidative, metal and protein stress responses upon HOCl stress are similar as outlined above between different bacteria cultivated in minimal medium (*B. subtilis*) versus RMPI (*S. aureus* and *S. pneumoniae*) (Chi et al., 2011; Loi et al., 2018), supporting that sub-lethal doses of HOCl reacted with the bacteria to similar extents without exerting non-physiological killing effects. However, further analyses will be required to evaluate the transcriptome signatures of the bacteria upon chloramine and HOCl treatment in comparison to clarify this question.

In addition, HOCl caused derepression of the CcpA regulon in *S. pneumoniae*, accompanied by induction of many regulons for the uptake and utilization of alternative carbohydrates, including the ScrR, FcsR, RafR, MalR, RegR, AgaR, XylR, BguR, GalR and LacR regulons (Minhas et al., 2021). While the basis for the CcpA derepression under HOCl in the pneumococcus is unknown, this study provides insights into the usage of alternative carbon sources under the growth conditions in supplemented RPMI medium. The XylR, GalR and LacR regulons for utilization and catabolism of lactose and galactose responded most strongly to HOCl stress, suggesting the switch from utilization of glucose to lactose (and the released galactose) via the Leloir and tagatose 6-phosphate pathways (Minhas et al., 2021). Galactose was shown to be the key sugar for niche adaptation to the nasopharynx and important for pneumococcal colonization (Paixao et al., 2015). However, whether this glucose-lactose/galactose switch is physiologically important to mediate protection against the oxidative burst during infections remains to be investigated in future studies.

Since the *nmlR-adhC* operon was most strongly upregulated under HOCl stress, the redox-sensing mechanism and functions of the MerR-family regulator NmlR were investigated in the pneumococcus. qRT-PCR analysis revealed that *adhC* transcription is most strongly elevated by aldehydes (Potter et al., 2010), HOCl, diamide and H₂O₂ stress in the pneumococcus. The ~8.5-fold higher induction rates of *adhC* transcription by sub-lethal 0.8 mM HOCl compared to that upon exposure to 0.45 mM H₂O₂ stress might be attributed to the different reactivities of both oxidants with Cys thiols. HOCl reacts with cysteine thiols according to second order rate constants of $k > 10^8 \text{ M}^{-1} \text{ s}^{-1}$ (Storkey et al., 2014), which is several magnitudes faster compared to the slow reaction of H₂O₂ with

biological thiols, determined as $k = 18\text{--}26 \text{ M}^{-1} \text{ s}^{-1}$ (Winterbourn & Metodiewa, 1999). In addition, *S. pneumoniae* produces millimolar levels of endogenous H₂O₂, which conferred resistance against exogenously encountered H₂O₂ (Mraheil et al., 2021), possibly explaining the lower response of the NmlR regulon towards H₂O₂. However, *adhC* was only weakly induced by the NO donor DEA-NONOate. Treatment of bacteria with the NO donor might cause a lower intracellular GSNO level compared to the external GSNO amount applied directly in the previous study (Stroeher et al., 2007). Transcriptional studies further showed that NmlR acts as activator of *adhC* transcription under HOCl stress, depending on the conserved Cys52 in vivo. The role of Cys52 of NmlR in redox-sensing was further confirmed in growth and survival assays under HOCl and H₂O₂ stress, since the *nmlRC52A* mutant was unable to restore the sensitive phenotypes of the $\Delta nmlR$ mutant back to the WT levels. Similarly, the conserved Cys was essential for aldehyde sensing in other MerR/NmlR homologs, including AdhR of *B. subtilis* (Nguyen et al., 2009) and NmlR of *H. influenzae* (Counago et al., 2016). In contrast, all four Cys residues were involved in transcriptional regulation of NmlR of *N. gonorrhoeae*, probably reflecting their role in Zn²⁺-binding (Kidd et al., 2005).

Using non-reducing SDS-PAGE and mass spectrometry, NmlR was shown to undergo a reversible thiol switch by formation of intersubunit disulfides or S-glutathionylation at Cys52 under oxidative stress in vitro. To estimate the position of Cys52, the structure of NmlR was modeled based on the template of the structure of the *L. monocytogenes* MerR homolog LMOF2365_2715 (PDB: 3gp4.1) using SWISS-MODEL (Biasini et al., 2014). In this NmlR model, the N-terminal $\alpha 1$ and $\alpha 2$ helices form the DNA-binding helix-turn-helix (HTH) motifs in each subunit, while the dimer interface is formed by the $\alpha 5$ helices. The Cys52 residues are located in the $\alpha 3$ helices and are ~27.8 Å apart in the dimeric structure, which is quite far away for disulfide bond formation (Figure S3). Thus, the S-glutathionylation model would be the more realistic redox-sensing mechanism under in vivo conditions, in agreement with the model for typical one-Cys-type redox-sensing regulators (Hillion & Antelmann, 2015; Lee et al., 2007).

Many MerR-type regulators were shown to be activated by conformational changes upon binding of inducers, resulting in re-orientation of the DNA-binding HTH motifs (Counago et al., 2016; Yang et al., 2021). The structural rearrangements of MerR-type regulators lead to realignments of the -35 and -10 promoter elements by introducing a kink in the DNA molecule to compensate for the overlong spacer of 19–20 bp, allowing the recognition by the RNAP to initiate transcription. Based on this overlong spacer, most MerR-family transcription factors, including pneumococcal NmlR, were shown to function as transcriptional activators in response to specific signals (Brown et al., 2003). However, NmlR might also function as repressor of *adhC* under control conditions, since transcription of *adhC* was upregulated in the $\Delta nmlR$ mutant. Similarly, other MerR-family transcription factors were postulated to switch from the repressor to the activator conformation in the presence of an inducer (Brown et al., 2003; Chang et al., 2015; Fang & Zhang, 2022).

However, the higher transcriptional activity without the MerR-type transcription factor might be also caused by the high promoter activity independent of the -35 element. Only upon MerR binding, this element was shown to be important for transcriptional initiation by the RNAP (Lund & Brown, 1989). Using the broccoli-FLAP assay, we could demonstrate that different NmlR thiol-switches, including the intermolecular disulfide and S-glutathionylated form, activate transcription initiation of the *nmlR-adhC* operon promoter by the heterologous *E. coli* σ^{70} -RNAP in vitro, while reduced NmlR rather inhibited transcription. Importantly, transcriptional activation by oxidized NmlR was dependent on Cys52, supporting the requirement of thiol-switches for NmlR regulation in vitro. The high basal transcription rate of the *nmlR* promoter by the *E. coli* σ^{70} -RNAP alone and the decreased transcription upon binding of reduced NmlR might also indicate its function as repressor under control conditions. Thus, our in vivo and in vitro transcriptional results might indicate that reduced NmlR acts as repressor under non-stress conditions, whereas thiol-oxidation of Cys52 to intersubunit disulfides and S-glutathionylations upon H_2O_2 and HOCl stress activates NmlR to induce the transcription of *adhC* by the RNAP. Although the broccoli-FLAP assay qualitatively reflects the proposed transcriptional activation mechanism of NmlR in vitro, we are aware that the transcription initiation rates are lower compared to the strong induction of *adhC* transcription upon HOCl stress in the qRT-PCR analyses in vivo. Thus, our in vitro assay does not fully recapitulate the transcriptional response in vivo. These discrepancies might be caused by the heterologous *E. coli* RNAP used for the broccoli-FLAP assay, which is not identical to pneumococcal RNAP and may lead to smaller effects of NmlR.

Overall, NmlR was identified as major redox-sensing regulator of the oxidative stress defense in *S. pneumoniae*. NmlR significantly improved the survival of *S. pneumoniae* D39 in the human macrophage cell line THP-1A. Decreased ROS and NO levels due to the addition of the flavoprotein inhibitor diphenyleneiodonium (DPI) significantly enhanced the intracellular survival of the $\Delta nmlR$ mutant inside macrophages (Altenhofer et al., 2015; O'Donnell et al., 1993; Stuehr et al., 1991). Thus, NmlR plays an important role in the virulence of *S. pneumoniae* by conferring resistance against the oxidative burst of activated immune cells during infections. The observed bacterial killing of the WT and the $\Delta nmlR$ mutant over time, even in the presence of DPI, is in agreement with previous findings that *S. pneumoniae* contributes to its cell death in the phagosome by endogenous H_2O_2 production (Mandell & Hook, 1969; Pitt & Bernheimer, 1974). Additionally, ROS and RNS production is thought to act in concert with changes in ion flux, pH decrease and hydrolytic enzymes in human macrophages to promote killing of the pathogen (Haas, 2007; Nüsse, 2011).

However, THP-1 macrophages do not express the myeloperoxidase to generate the highly microbicidal HOCl during the oxidative burst (Siraki, 2021). Thus, the NmlR regulon was shown here to confer protection only against ROS and RNS, but not against HOCl, during infections by THP-1A macrophages. In our future studies, the role of the NmlR regulon will be investigated

in the defense against MPO-produced HOCl during neutrophil infections. Nevertheless, the NmlR regulon contributed to the survival and replication of *S. pneumoniae* within macrophages, which is of major importance in its pathogenicity cycle. After colonization of the nasopharynx, *S. pneumoniae* can cause invasive infections and survive intracellularly within organs, such as the lung, spleen, heart and brain using different virulence factors and immune evasion mechanisms (Subramanian, Henriques-Normark, & Normark, 2019). In the lung, pneumococci are phagocytosed by mannose receptor C-type lectin 1 (MRC-1⁺) alveolar macrophages and replicate intracellularly by inhibition of lysosomal fusions and repression of inflammatory cytokine production (Subramanian, Neill, et al., 2019). In addition, CD169⁺ macrophages were identified as a reservoir for intracellular replication of pneumococci in the spleen, leading to bloodstream infections, such as septicaemia (Ercoli et al., 2018; Subramanian, Henriques-Normark, & Normark, 2019). Thus, it will be interesting to further study the mechanism of how AdhC promotes intracellular survival in different types of macrophages.

The NmlR-controlled alcohol dehydrogenase AdhC was identified as major defense mechanism against HOCl and H_2O_2 stress encountered during infections in *S. pneumoniae*. Alcohol-dehydrogenase 3 enzymes are widespread in bacteria and have been shown to catalyze detoxification of ω -hydroxy fatty acids, various aldehydes, medium-chain alcohols, GSNO and S-hydroxymethylglutathione (HMGSH) (Staab et al., 2008). In *N. meningitidis*, AdhC conferred protection against formaldehyde, but the $\Delta adhC$ mutant was not sensitive to methylglyoxal (Chen et al., 2013). The $\Delta adhC$ mutant of *H. influenzae* was unable to grow with high oxygen levels and displayed increased susceptibilities towards GSNO, methylglyoxal, glyceraldehyde and glycolaldehyde (Kidd et al., 2007, 2012), indicating also roles of other AdhC homologs in the oxidative and aldehyde stress defense. However, the $\Delta adhC$ mutant of *S. pneumoniae* did not show sensitive phenotypes under methylglyoxal and formaldehyde stress (Potter et al., 2010), raising the question of the physiological substrate of AdhC in *S. pneumoniae*.

Our results have shown that AdhC protects *S. pneumoniae* against HOCl and H_2O_2 stress, suggesting a direct or indirect role of AdhC in detoxification of these oxidants, which remains to be elucidated. Oxidants can react with various cellular macromolecules, resulting in reactive electrophilic species as secondary reactive species, such as quinones and aldehydes. Especially lipid peroxidation, DNA and sugar oxidation were shown to generate various aldehydes, including glyoxal, formaldehyde, and glycerine aldehyde (Beavers & Skaar, 2016; Marnett et al., 2003; Okado-Matsumoto & Fridovich, 2000; Spittler, 2008). Activated neutrophils contribute indirectly via HOCl production to the production of α -hydroxy and α,β -unsaturated aldehydes and other reactive species, highlighting the relevance of the redox sensor NmlR and the AdhC enzyme under infection conditions. Thus, our future analyses are directed to further investigate the redox-sensing and defense mechanisms of *S. pneumoniae* to mediate survival, replication and adaptation inside infected immune cells.

4 | EXPERIMENTAL PROCEDURES

4.1 | Bacterial strains, growth and survival assays

Bacterial strains and primers are listed in [Tables S3](#) and [S4](#). *E. coli* strains were cultivated in Luria Bertani (LB) medium for plasmid construction and protein expression. For growth and survival assays, *S. pneumoniae* strains were cultivated in supplemented RPMI medium as described previously (Schulz et al., 2014). At an optical density at 600nm (OD₆₀₀) of 0.4, the bacteria were exposed to different thiol-reactive compounds to monitor the growth and survival. Survival assays were performed by plating 100 µl of serial dilutions of *S. pneumoniae* strains onto Columbia blood agar plates for CFUs counting. Statistical analysis was performed using the Student's unpaired two-tailed t-test. The chemicals methylhydroquinone (MHQ), NaOCl, H₂O₂, diamide, methylglyoxal, formaldehyde and DEA-NONOate were purchased from Sigma Aldrich, Roth and Cayman Chemical Company, respectively. NaOCl dissociates in aqueous solution to hypochlorous acid (HOCl) and hypochlorite (OCl⁻) (Estrela et al., 2002). Thus, the concentration of HOCl was determined by absorbance measurements as described previously (Winter et al., 2008). DEA-NONOate was reported to dissociate to generate 1.5 M NO per 1 M of the parent compound (Keefer et al., 1996). Allicin was kindly provided by Martin Gruhlke and synthesized as described (Loi et al., 2019)

4.2 | Construction of the *S. pneumoniae* D39 $\Delta nmlR$ and $\Delta adhC$ mutant as well as the *nmlR*-, *nmlRC52A*- and *adhC*-complemented strains

The *S. pneumoniae* D39 *nmlR* (SPD_1637) and *adhC* (SPD_1636) deletion mutants were constructed by insertion-deletion mutagenesis as described previously (Hirschmann et al., 2021). For generation of the pSP72- $\Delta nmlR::ermB$ and pSP72- $\Delta adhC::ermB$ plasmids, the 5' and 3' flanking regions of both genes were amplified by PCR using primers *nmlR_fl_HindIII_for* and *nmlR_fl_BglII_rev* or *adhC_fl_HindIII_for* and *adhC_fl_BglII_rev*, respectively ([Table S4](#)). The PCR products were digested with *HindIII* and *BglII* and cloned into plasmid pSP72. The recombinant plasmids were used as a template for an inverse PCR with primers *nmlR_in_Sall_for* and *nmlR_in_BamHI_rev* or *adhC_in_Sall_for* and *adhC_in_BamHI_rev*, respectively ([Table S4](#)). The resulting PCR products were digested with *BamHI* and *Sall* and ligated with the *erm*^R cassette, which was amplified with the primers *Ery_BamHI_for* and *Ery_Sall_rev* from the plasmid pTP1. The generated plasmids were transferred into *S. pneumoniae* D39 WT as described previously (Gomez-Mejia et al., 2018). Briefly, the bacteria were cultivated in THY-medium until an OD₆₀₀ of 0.1. The transformation was induced by addition of the competence-stimulating peptide 1 (CSP1) and the pSP72- $\Delta nmlR::ermB$ and pSP72- $\Delta adhC::ermB$ plasmids. The bacteria were exposed to a cold shock for 10 min, followed by 30 min incubation at 30°C. Bacteria were grown for 2 h

at 37°C and plated onto Columbia blood agar plates containing erythromycin for selection.

For construction of the *S. pneumoniae* D39 *nmlR* and *adhC*-complemented strains, the coding sequences were amplified from chromosomal DNA using the primers *nmlR_pBAV_for_NcoI* and *nmlR_pBAV_rev_HindIII* or *adhC_pBAV_for_NcoI* and *adhC_pBAV_rev_HindIII* ([Table S4](#)). To generate the plasmid for construction of the *nmlRC52A*-complemented strain, two first-round PCR products, obtained with the primer pairs *NmlRC52A_f2_for* and *nmlR_pBAV_rev_HindIII* as well as *NmlRC52A_f1_rev* and *nmlR_pBAV_for_NcoI*, were hybridized and amplified by a second round of PCR using the primers *nmlR_pBAV_for_NcoI* and *nmlR_pBAV_rev_HindIII*, as described previously (Loi et al., 2018). The purified PCR products were digested with *NcoI* and *HindIII* and ligated into plasmid pBAV1CpE (Hess et al., 2017), which was kindly provided by Sven Hammerschmidt (University of Greifswald). The resulting plasmids pBAV-*nmlR*, pBAV-*nmlRC52A* and pBAV-*adhC* ([Table S3](#)) were introduced into the corresponding *S. pneumoniae* D39 $\Delta nmlR$ and $\Delta adhC$ mutants as described above. Transformants were selected on Columbia blood agar plates containing erythromycin and chloramphenicol. In these complemented strains, *nmlR*, *nmlRC52A* and *adhC* are ectopically and constitutively expressed from an erythromycin promoter (pE).

4.3 | RNA isolation, RNA-seq transcriptomics and qRT-PCR analysis

S. pneumoniae strains were cultivated in RPMI medium and treated with various thiol-reactive compounds at an OD₆₀₀ of 0.4 for 30 min. Bacteria were harvested in ice-cold killing buffer (50mM Tris pH 7.5, 5mM MgCl₂, 20mM NaN₃), centrifuged at 4750rpm for 10 min at 4°C and the pellets were immediately frozen in liquid nitrogen and stored at -80°C. RNA isolation was performed using an acidic phenol-chloroform extraction protocol (Wetzstein et al., 1992). After DNase-I treatment (Zymo Research, Germany), the RNA quality was checked by Trinean Xpose (Gentbrugge, Belgium) and the Agilent RNA Nano 6000 kit using an Agilent 2100 Bioanalyzer (Agilent Technologies, Böblingen, Germany). For RNA-seq transcriptomics, Ribo-Zero rRNA Removal Kit (Bacteria) from Illumina (San Diego, CA, USA) was used to remove the rRNA. TruSeq Stranded mRNA Library Prep Kit from Illumina (San Diego, CA, United States) was applied to prepare the cDNA libraries. The cDNAs were sequenced paired end on an Illumina HiSeq 1500 (San Diego, CA, United States) using 70 and 75bp read length and a minimum sequencing depth of 10 million reads per library. The transcriptome sequencing raw data files are available in the ArrayExpress database (www.ebi.ac.uk/arrayexpress) under accession number E-MTAB-11968.

For quantitative Real-Time PCR (qRT-PCR) analysis, the purified total RNA was reverse-transcribed into cDNA using the High-capacity cDNA reverse transcription kit (Applied Biosystems, USA) according to the recommendations of the manufacturer. SYBR™ GreenER™ (Applied Biosystems, USA) intercalation in

double-stranded DNA was measured using a 7300 Real-Time PCR System (Applied Biosystems, USA) according to the manufacturer's instructions. The amplification primer pair is listed in Table S4. The verification of the resulting qRT-PCR products was performed by melting curve analysis. The crossing points were determined using the Sequence Detection Software Version 1.4 (Applied Biosystems, USA) and the differences in gene expression were analyzed by comparing the crossing points of the samples measured in duplicate as described previously (Busche et al., 2012).

4.4 | Cloning, expression and purification of His-tagged NmlR and NmlRC52A proteins in *E. coli*

To generate the plasmids pET11b-*nmlR* and pET11b-*nmlRC52A*, the *nmlR* gene (SPD_1637) was amplified from chromosomal DNA of *S. pneumoniae* D39 or from the pBAV-*nmlRC52A* plasmid, respectively, using primers *nmlR*_pET_NheI_for and *nmlR*_pET_BamHI_rev (Table S4). The PCR products were digested with *NheI* and *BamHI* and inserted into plasmid pET11b (Novagen) (Table S3). For expression and purification of His-tagged NmlR and NmlRC52A, *E. coli* BL21(DE3)*plysS* with plasmids pET11b-*nmlR* and pET11b-*nmlRC52A* were cultivated in 1.5 L LB medium until the exponential growth phase at an OD₆₀₀ of 0.7, followed by addition of 1 mM iso-propyl-β-D-thiogalactopyranoside (IPTG) for 5 h at 30°C. Recombinant His-tagged proteins were purified using His Trap™ HP Ni-NTA columns and the ÄKTA purifier liquid chromatography system as described (Loi et al., 2018).

4.5 | Electrophoretic mobility shift assays (EMSAs) of NmlR and NmlRC52A proteins

For EMSAs, the 274 bp DNA fragment containing the upstream region of *nmlR* was amplified by PCR (Table S4). The DNA-binding reactions were performed with 15 ng of the promoter region and purified His-tagged NmlR and NmlRC52A proteins for 45 min, as described previously (Loi et al., 2018). Diamide was added to the DNA-NmlR-complex for 30 min to observe the dissociation of NmlR from the DNA. To generate two base substitutions in each half of the inverted repeat, two first-round PCRs were performed using the primer pairs EMSA_*nmlR*_m1_for, EMSA_*nmlR*_rev and EMSA_*nmlR*_m1_rev, EMSA_*nmlR*_for or EMSA_*nmlR*_m2_for, EMSA_*nmlR*_rev and EMSA_*nmlR*_m2_rev, EMSA_*nmlR*_for, respectively (Table S4). The first round PCR products were hybridized and amplified by a second round of PCR using the primers EMSA_*nmlR*_for and EMSA_*nmlR*_rev.

4.6 | Multiround in vitro transcription assay to monitor transcription initiation rates using broccoli-FLAP assay

To determine regulatory effects of NmlR on transcription initiation of σ^{70} -RNAP, broccoli-FLAP assay was performed as described

(Huang et al., 2022) with slight variations. In short, the broccoli gene was placed under control of the *S. pneumoniae nmlR* promoter region (CTTGACTTGGAGTCAACTCAAAGTTATATAATAAGATAA) (Stroeher et al., 2007) in pOP005 (<https://benchling.com/s/seq-5bEIoESV96X1uEPcEWOW>). *E. coli* RNAP and *E. coli* σ^{70} were purified as described before (Said et al., 2017). To monitor transcription, *E. coli* RNAP and σ^{70} were incubated for 30 min at 30°C to form the holoenzyme. 2 μ M holoenzyme were mixed with 50 nM plasmid DNA and 10 μ M DFHBI-1T in transcription buffer (10 mM Tris pH 7.9, 10 mM MgCl₂, 100 mM KCl) and transcription was started by adding an equal volume of 1 mM pre-warmed rNTPs to the reaction and quick mixing. The sample was placed in an OptiPlate™ 384-well plate (PerkinElmer) and fluorescence was measured using a Spark Multimode Microplate reader (Tecan). Fluorescence was monitored every second for a total duration of 3 min using an excitation wavelength of 472 nm and an emission wavelength of 507 nm. Where indicated, 10 μ M of NmlR or NmlRC52A proteins were added to the transcription reaction prior to rNTP addition and incubated for 5 min at room temperature. The NmlR_{red} and NmlRC52A_{red} proteins were reduced with 10 mM TCEP for 30 min at room temperature. The oxidized NmlR_{ox}, C52A_{ox}, NmlR_{GSH} and C52A_{GSH} proteins were generated by first reducing NmlR and NmlRC52A with 10 mM DTT, followed by buffer exchange, and oxidation with an equal volume of a 2.5% H₂O₂ (w/v) solution in the absence (NmlR_{ox}, C52A_{ox}) or presence of 0.3 mM GSH (NmlR_{GSH}, C52A_{GSH}) for 15 min at room temperature. To neutralize the reaction, 1/10 V of a saturated solution of sodium bicarbonate was added to the reaction followed by buffer exchange. All measurements were performed in triplicates. Initial transcription rates were calculated from the slope of the initial linear increase in fluorescence after the corresponding lag phases (t_0 , determined from the graph; linear phase measured for all samples from $t_1 = 50$ s to $t_2 = 100$ s). Means and SDs were calculated using Prism software (GraphPad; RRID: SCR_002798). Relative initiation rates were determined by correlating initial transcription rates to the rates of RNAP, which was set to 1. *p* values were calculated using Excel (Microsoft) based on unpaired, two-sided *t* tests. For graphical representations, Y0 values were subtracted so that the curves start at 0 relative fluorescence.

4.7 | Identification of thiol-modifications of the NmlR protein in vitro

To study thiol-oxidation of the NmlR protein in vitro, the purified protein was reduced with 10 mM DTT for 15 min and oxidized with increasing amounts of diamide, HOCL and H₂O₂ for 15 min. Free thiols were alkylated with 50 mM iodoacetamide (IAM) for 30 min in the dark before samples were subjected to non-reducing SDS-PAGE analyses. The post-translational thiol-modifications of oxidized NmlR (with or without GSH) were determined by matrix-assisted laser desorption ionization-time of flight mass spectrometry (MALDI-TOF-MS) using an Ultraflex-II TOF/TOF instrument (Bruker Daltonics, Bremen, Germany) equipped with a 200 Hz

solid-state Smart beam™ laser. The bands of reduced and oxidized NmIR from the non-reducing SDS-PAGE were in-gel digested with trypsin as described previously (Chi et al., 2011). Alpha-Cyano-4-hydroxycinnamic acid was used as matrix substance and the mass spectrometer was operated in the positive reflector mode. Mass spectra were acquired over an *m/z* range of 400–4000.

4.8 | Macrophage infection assays

The infection assays were performed as reported previously (Kohler et al., 2016), using the human macrophage cell line THP-1A, an adherent derivative of the THP-1 cell line (Van Immerseel et al., 2003). The cells were cultivated in Iscove's modified Dulbecco's medium (Biocrom) with 10% heat-inactivated fetal bovine serum (FBS) at 37°C and 5% CO₂. Two days before the infection experiment, the cells were seeded at densities of 1 × 10⁵ cells/ml in 48-well TC-plates (Sarstedt, Germany). If indicated, 5 μM of the flavoprotein inhibitor diphenyleneiodonium (DPI) was added 16 hours prior infection. On the day of infection, *S. pneumoniae* strains were grown in supplemented RPMI medium to an OD₆₀₀ of 0.35. Macrophages were infected with log phase bacteria at a multiplicity of infection (MOI) of 1:50. One hour after infection, the cell culture medium was replaced and 100 μg/ml gentamicin and 100 U/ml penicillin G were added for 1 h to kill extracellular bacteria. The intracellular survival of the bacteria was determined at different time points, including 135, 150, 180, 240 and 300 min after phagocytosis. Infected macrophages were lysed with 1% saponin and the supernatant with internalized intracellular bacteria was plated on Columbia blood agar plates for determination of CFUs. The percentage of survival of the bacteria post infection was calculated in comparison to the CFU counts at the 2 h time point post infection, which was set to 100% as indicated in the figure legend.

AUTHOR CONTRIBUTIONS

Verena Nadin Fritsch: Conceptualization; data curation; formal analysis; investigation; methodology; validation; visualization; writing – original draft; writing – review and editing. **Nico Linzner:** Formal analysis; investigation; methodology; validation; writing – review and editing. **Tobias Busche:** Data curation; formal analysis; methodology; software; validation; visualization; writing – review and editing. **Nelly Said:** Data curation; formal analysis; investigation; methodology; software; validation; writing – review and editing. **Christoph Weise:** Data curation; formal analysis; methodology; software; validation; writing – review and editing. **Jörn Kalinowski:** Data curation; formal analysis; methodology; software; validation; writing – review and editing. **Markus C. Wahl:** Data curation; formal analysis; methodology; software; supervision; validation; writing – review and editing. **Haike Antelmann:** Conceptualization; data curation; funding acquisition; project administration; resources; supervision; validation; visualization; writing – original draft; writing – review and editing.

ACKNOWLEDGMENTS

This work was supported by grants from the Deutsche Forschungsgemeinschaft (DFG) of the SPP1710 (AN746/4-1 and AN746/4-2), SFB973 (project C08) and TR84 (project B06) to H.A. The experiments related to the in vitro transcription assay at the *nmIR* promoter were further supported by the DFG grant WA 1126/11-1 (project number 433623608) to M.C.W. For mass spectrometry performed by C.W., we would like to acknowledge the assistance of the Core Facility BioSupraMol supported by the DFG. We are grateful to Sven Hammerschmidt (University of Greifswald) for providing the pBAV1CpE plasmid and to Doris Frey (Charité-Universitätsmedizin, Berlin) for the technical assistance with the qRT-PCR analyses. We further thank Martin Clemens Horst Gruhlke and Alan John Slusarenko (RWTH Aachen University, Department of Plant Physiology) for providing alliin.





CONFLICT OF INTEREST

No competing financial interests exist.

DATA AVAILABILITY STATEMENT

The transcriptome sequencing raw data files are available in the ArrayExpress database (www.ebi.ac.uk/arrayexpress) under accession number E-MTAB-11968. All other data are available in the manuscript figures or supplemental material.

ORCID

Verena Nadin Fritsch  <https://orcid.org/0000-0002-7598-6754>
 Tobias Busche  <https://orcid.org/0000-0001-9211-8927>
 Nelly Said  <https://orcid.org/0000-0001-8352-5555>
 Christoph Weise  <https://orcid.org/0000-0002-5507-4694>
 Jörn Kalinowski  <https://orcid.org/0000-0002-9052-1998>
 Markus C. Wahl  <https://orcid.org/0000-0002-2811-5307>
 Haike Antelmann  <https://orcid.org/0000-0002-1766-4386>

REFERENCES

- Altenhofer, S., Radermacher, K.A., Kleikers, P.W., Wingler, K. & Schmidt, H.H. (2015) Evolution of NADPH oxidase inhibitors: selectivity and mechanisms for target engagement. *Antioxidants & Redox Signaling*, 23, 406–427.
- Ashby, L.V., Springer, R., Hampton, M.B., Kettle, A.J. & Winterbourn, C.C. (2020) Evaluating the bactericidal action of hypochlorous acid in culture media. *Free Radical Biology & Medicine*, 159, 119–124.
- Barrette, W.C., Jr., Hannum, D.M., Wheeler, W.D. & Hurst, J.K. (1989) General mechanism for the bacterial toxicity of hypochlorous acid: abolition of ATP production. *Biochemistry*, 28, 9172–9178.
- Beavers, W.N. & Skaar, E.P. (2016) Neutrophil-generated oxidative stress and protein damage in *Staphylococcus aureus*. *Pathogens and Disease*, 74, ftw060.
- Biasini, M., Bienert, S., Waterhouse, A., Arnold, K., Studer, G., Schmidt, T. et al. (2014) SWISS-MODEL: modelling protein tertiary and quaternary structure using evolutionary information. *Nucleic Acids Research*, 42, W252–W258.
- Brown, N.L., Stoyanov, J.V., Kidd, S.P. & Hobman, J.L. (2003) The MerR family of transcriptional regulators. *FEMS Microbiology Reviews*, 27, 145–163.

- Busche, T., Silar, R., Picmanova, M., Patek, M. & Kalinowski, J. (2012) Transcriptional regulation of the operon encoding stress-responsive ECF sigma factor SigH and its anti-sigma factor RshA, and control of its regulatory network in *Corynebacterium glutamicum*. *BMC Genomics*, 13, 445.
- CDC. (2020) Pneumococcal disease.
- Chandrangu, P., Dusi, R., Hamilton, C.J. & Helmann, J.D. (2014) Methylglyoxal resistance in *Bacillus subtilis*: contributions of bacillithiol-dependent and independent pathways. *Molecular Microbiology*, 91, 706–715.
- Chang, C.C., Lin, L.Y., Zou, X.W., Huang, C.C. & Chan, N.L. (2015) Structural basis of the mercury(II)-mediated conformational switching of the dual-function transcriptional regulator MerR. *Nucleic Acids Research*, 43, 7612–7623.
- Chapuy-Regaud, S., Ogunniyi, A.D., Diallo, N., Huet, Y., Desnottes, J.F., Paton, J.C. et al. (2003) RegR, a global LacI/GalR family regulator, modulates virulence and competence in *Streptococcus pneumoniae*. *Infection and Immunity*, 71, 2615–2625.
- Chen, N.H., Counago, R.M., Djoko, K.Y., Jennings, M.P., Apicella, M.A., Kobe, B. et al. (2013) A glutathione-dependent detoxification system is required for formaldehyde resistance and optimal survival of *Neisseria meningitidis* in biofilms. *Antioxidants & Redox Signaling*, 18, 743–755.
- Chi, B.K., Gronau, K., Mäder, U., Hessling, B., Becher, D. & Antelmann, H. (2011) S-bacillithiolation protects against hypochlorite stress in *Bacillus subtilis* as revealed by transcriptomics and redox proteomics. *Molecular & Cellular Proteomics*, 10, M111 009506.
- Counago, R.M., Chen, N.H., Chang, C.W., Djoko, K.Y., McEwan, A.G. & Kobe, B. (2016) Structural basis of thiol-based regulation of formaldehyde detoxification in *H. influenzae* by a MerR regulator with no sensor region. *Nucleic Acids Research*, 44, 6981–6993.
- Dupuy, E. & Collet, J.F. (2021) Fort CnoX: protecting bacterial proteins from misfolding and oxidative damage. *Frontiers in Molecular Biosciences*, 8, 681932.
- Ercoli, G., Fernandes, V.E., Chung, W.Y., Wanford, J.J., Thomson, S., Bayliss, C.D. et al. (2018) Intracellular replication of *Streptococcus pneumoniae* inside splenic macrophages serves as a reservoir for septicaemia. *Nature Microbiology*, 3, 600–610.
- Estrela, C., Estrela, C.R.A., Barbin, E.L., Spanó, J.C.E., Marchesan, M.A. & Pécora, J.D. (2002) Mechanism of action of sodium hypochlorite. *Brazilian Dental Journal*, 13, 113–117.
- Fang, C. & Zhang, Y. (2022) Bacterial MerR family transcription regulators: activation by distortion. *Acta Biochimica et Biophysica Sinica (Shanghai)*, 54, 25–36.
- Filonov, G.S., Moon, J.D., Svensen, N. & Jaffrey, S.R. (2014) Broccoli: rapid selection of an RNA mimic of green fluorescent protein by fluorescence-based selection and directed evolution. *Journal of the American Chemical Society*, 136, 16299–16308.
- Fliss, H. & Menard, M. (1991) Hypochlorous acid-induced mobilization of zinc from metalloproteins. *Archives of Biochemistry and Biophysics*, 287, 175–179.
- Gennaris, A. & Collet, J.F. (2013) The 'captain of the men of death', *Streptococcus pneumoniae*, fights oxidative stress outside the 'city wall'. *EMBO Molecular Medicine*, 5, 1798–1800.
- Gomez-Mejia, A., Gamez, G., Hirschmann, S., Kluger, V., Rath, H., Bohm, S. et al. (2018) Pneumococcal metabolic adaptation and colonization are regulated by the two-component regulatory system O8. *mSphere*, 3, e00165-18.
- Gray, M.J., Wholey, W.Y. & Jakob, U. (2013) Bacterial responses to reactive chlorine species. *Annual Review of Microbiology*, 67, 141–160.
- Haas, A. (2007) The phagosome: compartment with a license to kill. *Traffic*, 8, 311–330.
- Hess, N., Waldow, F., Kohler, T.P., Rohde, M., Kreikemeyer, B., Gomez-Mejia, A. et al. (2017) Lipoteichoic acid deficiency permits normal growth but impairs virulence of *Streptococcus pneumoniae*. *Nature Communications*, 8, 2093.
- Hillion, M. & Antelmann, H. (2015) Thiol-based redox switches in prokaryotes. *Biological Chemistry*, 396, 415–444.
- Hillion, M., Bernhardt, J., Busche, T., Rossius, M., Maass, S., Becher, D. et al. (2017) Monitoring global protein thiol-oxidation and protein S-mycothiolation in *Mycobacterium smegmatis* under hypochlorite stress. *Scientific Reports*, 7, 1195.
- Hirschmann, S., Gomez-Mejia, A., Mader, U., Karsunke, J., Driesch, D., Rohde, M. et al. (2021) The two-component system O9 regulates pneumococcal carbohydrate metabolism and capsule expression. *Microorganisms*, 9, 468.
- Hobman, J.L., Wilkie, J. & Brown, N.L. (2005) A design for life: prokaryotic metal-binding MerR family regulators. *Biometals*, 18, 429–436.
- Huang, Y.H., Trapp, V., Puro, O., Makinen, J.J., Metsa-Ketela, M., Wahl, M.C. et al. (2022) Fluorogenic RNA aptamers to probe transcription initiation and co-transcriptional RNA folding by multi-subunit RNA polymerases. *Methods in Enzymology*, 675, 207–233.
- Keefer, L.K., Nims, R.W., Davies, K.M. & Wink, D.A. (1996) "NONOates" (1-substituted diazen-1-ium-1,2-diolates) as nitric oxide donors: convenient nitric oxide dosage forms. *Methods in Enzymology*, 268, 281–293.
- Kidd, S.P., Jiang, D., Jennings, M.P. & McEwan, A.G. (2007) Glutathione-dependent alcohol dehydrogenase AdhC is required for defense against nitrosative stress in *Haemophilus influenzae*. *Infection and Immunity*, 75, 4506–4513.
- Kidd, S.P., Jiang, D., Tikhomirova, A., Jennings, M.P. & McEwan, A.G. (2012) A glutathione-based system for defense against carbonyl stress in *Haemophilus influenzae*. *BMC Microbiology*, 12, 159.
- Kidd, S.P., Potter, A.J., Apicella, M.A., Jennings, M.P. & McEwan, A.G. (2005) NmlR of *Neisseria gonorrhoeae*: a novel redox responsive transcription factor from the MerR family. *Molecular Microbiology*, 57, 1676–1689.
- Kloosterman, T.G., van der Kooi-Pol, M.M., Bijlsma, J.J. & Kuipers, O.P. (2007) The novel transcriptional regulator SczA mediates protection against Zn²⁺ stress by activation of the Zn²⁺-resistance gene *czcD* in *Streptococcus pneumoniae*. *Molecular Microbiology*, 65, 1049–1063.
- Kohler, T.P., Scholz, A., Kiachludis, D. & Hammerschmidt, S. (2016) Induction of central host signaling kinases during pneumococcal infection of human THP-1 cells. *Frontiers in Cellular and Infection Microbiology*, 6, 48.
- Lee, J.W., Soonsanga, S. & Helmann, J.D. (2007) A complex thiolate switch regulates the *Bacillus subtilis* organic peroxide sensor OhrR. *Proceedings of the National Academy of Sciences of the United States of America*, 104, 8743–8748.
- Loi, V.V., Busche, T., Tedin, K., Bernhardt, J., Wollenhaupt, J., Huyen, N.T.T. et al. (2018) Redox-sensing under hypochlorite stress and infection conditions by the Rrf2-family repressor HypR in *Staphylococcus aureus*. *Antioxidants & Redox Signaling*, 29, 615–636.
- Loi, V.V., Huyen, N.T.T., Busche, T., Tung, Q.N., Gruhlke, M.C.H., Kalinowski, J. et al. (2019) *Staphylococcus aureus* responds to alliin by global S-thioallylation—role of the Brx/BSH/YpdA pathway and the disulfide reductase MerA to overcome alliin stress. *Free Radical Biology & Medicine*, 139, 55–69.
- Love, M.I., Huber, W. & Anders, S. (2014) Moderated estimation of fold change and dispersion for RNA-seq data with DESeq2. *Genome Biology*, 15, 550.
- Lund, P.A. & Brown, N.L. (1989) Regulation of transcription in *Escherichia coli* from the *mer* and *merR* promoters in the transposon Tn501. *Journal of Molecular Biology*, 205, 343–353.
- Lv, J., He, X., Wang, H., Wang, Z., Kelly, G.T., Wang, X. et al. (2017) TLR4-NOX2 axis regulates the phagocytosis and killing of *Mycobacterium tuberculosis* by macrophages. *BMC Pulmonary Medicine*, 17, 194.
- Ma, Z., Chandrangu, P., Helmann, T.C., Romsang, A., Gaballa, A. & Helmann, J.D. (2014) Bacillithiol is a major buffer of the labile zinc pool in *Bacillus subtilis*. *Molecular Microbiology*, 94, 756–770.

- Mandell, G.L. & Hook, E.W. (1969) Leukocyte bactericidal activity in chronic granulomatous disease: correlation of bacterial hydrogen peroxide production and susceptibility to intracellular killing. *Journal of Bacteriology*, *100*, 531–532.
- Marnett, L.J., Riggins, J.N. & West, J.D. (2003) Endogenous generation of reactive oxidants and electrophiles and their reactions with DNA and protein. *The Journal of Clinical Investigation*, *111*, 583–593.
- Martin, J.E., Edmonds, K.A., Bruce, K.E., Campanello, G.C., Eijkelkamp, B.A., Brazel, E.B. et al. (2017) The zinc efflux activator SczA protects *Streptococcus pneumoniae* serotype 2 D39 from intracellular zinc toxicity. *Molecular Microbiology*, *104*, 636–651.
- McEwan, A.G., Djoko, K.Y., Chen, N.H., Counago, R.L., Kidd, S.P., Potter, A.J. et al. (2011) Novel bacterial MerR-like regulators their role in the response to carbonyl and nitrosative stress. *Advances in Microbial Physiology*, *58*, 1–22.
- Minhas, V., Paton, J.C. & Trappetti, C. (2021) Sickly sweet—how sugar utilization impacts pneumococcal disease progression. *Trends in Microbiology*, *29*, 768–771.
- Moore, C.M., Gaballa, A., Hui, M., Ye, R.W. & Helmann, J.D. (2005) Genetic and physiological responses of *Bacillus subtilis* to metal ion stress. *Molecular Microbiology*, *57*, 27–40.
- Mraheil, M.A., Toque, H.A., La Pietra, L., Hamacher, J., Phanthok, T., Verin, A. et al. (2021) Dual role of hydrogen peroxide as an oxidant in *Pneumococcal pneumonia*. *Antioxidants & Redox Signaling*, *34*, 962–978.
- Nguyen, T.T., Eiamphungporn, W., Mäder, U., Liebecke, M., Lalk, M., Hecker, M. et al. (2009) Genome-wide responses to carbonyl electrophiles in *Bacillus subtilis*: control of the thiol-dependent formaldehyde dehydrogenase AdhA and cysteine proteinase YraA by the MerR-family regulator YraB (AdhR). *Molecular Microbiology*, *71*, 876–894.
- Nüsse, O. (2011) Biochemistry of the phagosome: the challenge to study a transient organelle. *TheScientificWorldJournal*, *11*, 2364–2381.
- O'Donnell, B.V., Tew, D.G., Jones, O.T. & England, P.J. (1993) Studies on the inhibitory mechanism of iodonium compounds with special reference to neutrophil NADPH oxidase. *The Biochemical Journal*, *290*(Pt 1), 41–49.
- Okado-Matsumoto, A. & Fridovich, I. (2000) The role of alpha, beta-dicarbonyl compounds in the toxicity of short chain sugars. *The Journal of Biological Chemistry*, *275*, 34853–34857.
- Paixao, L., Oliveira, J., Verissimo, A., Vinga, S., Lourenco, E.C., Ventura, M.R. et al. (2015) Host glycan sugar-specific pathways in *Streptococcus pneumoniae*: galactose as a key sugar in colonisation and infection [corrected]. *PLoS One*, *10*, e0121042.
- Pericone, C.D., Park, S., Imlay, J.A. & Weiser, J.N. (2003) Factors contributing to hydrogen peroxide resistance in *Streptococcus pneumoniae* include pyruvate oxidase (SpxB) and avoidance of the toxic effects of the Fenton reaction. *Journal of Bacteriology*, *185*, 6815–6825.
- Peskin, A.V. & Winterbourn, C.C. (2001) Kinetics of the reactions of hypochlorous acid and amino acid chloramines with thiols, methionine, and ascorbate. *Free Radical Biology & Medicine*, *30*, 572–579.
- Pitt, J. & Bernheimer, H.P. (1974) Role of peroxide in phagocytic killing of pneumococci. *Infection and Immunity*, *9*, 48–52.
- Potter, A.J., Kidd, S.P., McEwan, A.G. & Paton, J.C. (2010) The MerR/NmlR family transcription factor of *Streptococcus pneumoniae* responds to carbonyl stress and modulates hydrogen peroxide production. *Journal of Bacteriology*, *192*, 4063–4066.
- Said, N., Krupp, F., Anechenko, E., Santos, K.F., Dybkov, O., Huang, Y.H. et al. (2017) Structural basis for lambdaN-dependent processive transcription antitermination. *Nature Microbiology*, *2*, 17062.
- Saleh, M., Bartual, S.G., Abdullah, M.R., Jensch, I., Asmat, T.M., Petruschka, L. et al. (2013) Molecular architecture of *Streptococcus pneumoniae* surface thioredoxin-fold lipoproteins crucial for extracellular oxidative stress resistance and maintenance of virulence. *EMBO Molecular Medicine*, *5*, 1852–1870.
- Schulz, C., Gierok, P., Petruschka, L., Lalk, M., Mader, U. & Hammerschmidt, S. (2014) Regulation of the arginine deiminase system by ArgR2 interferes with arginine metabolism and fitness of *Streptococcus pneumoniae*. *mBio*, *5*, e01858-14.
- Shafeeq, S., Yesilkaya, H., Kloosterman, T.G., Narayanan, G., Wandel, M., Andrew, P.W. et al. (2011) The *cop* operon is required for copper homeostasis and contributes to virulence in *Streptococcus pneumoniae*. *Molecular Microbiology*, *81*, 1255–1270.
- Siraki, A.G. (2021) The many roles of myeloperoxidase: from inflammation and immunity to biomarkers, drug metabolism and drug discovery. *Redox Biology*, *46*, 102109.
- Spiteller, G. (2008) Peroxyl radicals are essential reagents in the oxidation steps of the Maillard reaction leading to generation of advanced glycation end products. *Annals of the New York Academy of Sciences*, *1126*, 128–133.
- Staab, C.A., Hellgren, M. & Hoog, J.O. (2008) Medium- and short-chain dehydrogenase/reductase gene and protein families: dual functions of alcohol dehydrogenase 3: implications with focus on formaldehyde dehydrogenase and S-nitrosoglutathione reductase activities. *Cellular and Molecular Life Sciences*, *65*, 3950–3960.
- Storkey, C., Davies, M.J. & Pattison, D.I. (2014) Reevaluation of the rate constants for the reaction of hypochlorous acid (HOCl) with cysteine, methionine, and peptide derivatives using a new competition kinetic approach. *Free Radical Biology & Medicine*, *73*, 60–66.
- Stroehrer, U.H., Kidd, S.P., Stafford, S.L., Jennings, M.P., Paton, J.C. & McEwan, A.G. (2007) A pneumococcal MerR-like regulator and S-nitrosoglutathione reductase are required for systemic virulence. *The Journal of Infectious Diseases*, *196*, 1820–1826.
- Stuehr, D.J., Fasehun, O.A., Kwon, N.S., Gross, S.S., Gonzalez, J.A., Levi, R. et al. (1991) Inhibition of macrophage and endothelial cell nitric oxide synthase by diphenyleneiodonium and its analogs. *The FASEB Journal*, *5*, 98–103.
- Subramanian, K., Henriques-Normark, B. & Normark, S. (2019) Emerging concepts in the pathogenesis of the *Streptococcus pneumoniae*: from nasopharyngeal colonizer to intracellular pathogen. *Cellular Microbiology*, *21*, e13077.
- Subramanian, K., Neill, D.R., Malak, H.A., Spelmink, L., Khandaker, S., Dalla Libera Marchiori, G. et al. (2019) Pneumolysin binds to the mannose receptor C type 1 (MRC-1) leading to anti-inflammatory responses and enhanced pneumococcal survival. *Nature Microbiology*, *4*, 62–70.
- Supa-Amornkul, S., Chantratita, W., Srichunrusami, C., Janchompoo, P. & Chaturongakul, S. (2016) *Listeria monocytogenes* MerR-like regulator NmlRlm: its transcriptome and role in stress response. *Foodborne Pathogens and Disease*, *13*, 369–378.
- Ulfing, A. & Leichert, L.I. (2021) The effects of neutrophil-generated hypochlorous acid and other hypohalous acids on host and pathogens. *Cellular and Molecular Life Sciences*, *78*, 385–414.
- Van Immerseel, F., De Buck, J., Pasmans, F., Velge, P., Bottreau, E., Fievez, V. et al. (2003) Invasion of *Salmonella enteritidis* in avian intestinal epithelial cells in vitro is influenced by short-chain fatty acids. *International Journal of Food Microbiology*, *85*, 237–248.
- Wetzstein, M., Volker, U., Dedio, J., Lobau, S., Zuber, U., Schiesswohl, M. et al. (1992) Cloning, sequencing, and molecular analysis of the *dnaK* locus from *Bacillus subtilis*. *Journal of Bacteriology*, *174*, 3300–3310.
- Winter, J., Ilbert, M., Graf, P.C., Ozcelik, D. & Jakob, U. (2008) Bleach activates a redox-regulated chaperone by oxidative protein unfolding. *Cell*, *135*, 691–701.
- Winterbourn, C.C. & Kettle, A.J. (2013) Redox reactions and microbial killing in the neutrophil phagosome. *Antioxidants & Redox Signaling*, *18*, 642–660.
- Winterbourn, C.C., Kettle, A.J. & Hampton, M.B. (2016) Reactive oxygen species and neutrophil function. *Annual Review of Biochemistry*, *85*, 765–792.

- Winterbourn, C.C. & Metodiewa, D. (1999) Reactivity of biologically important thiol compounds with superoxide and hydrogen peroxide. *Free Radical Biology & Medicine*, 27, 322–328.
- Yang, Y., Liu, C., Zhou, W., Shi, W., Chen, M., Zhang, B. et al. (2021) Structural visualization of transcription activated by a multidrug-sensing MerR family regulator. *Nature Communications*, 12, 2702.
- Yesilkaya, H., Andisi, V.F., Andrew, P.W. & Bijlsma, J.J. (2013) *Streptococcus pneumoniae* and reactive oxygen species: an unusual approach to living with radicals. *Trends in Microbiology*, 21, 187–195.
- Zhang, Y., Martin, J.E., Edmonds, K.A., Winkler, M.E. & Giedroc, D.P. (2022) SifR is an Rrf2-family quinone sensor associated with catechol iron uptake in *Streptococcus pneumoniae* D39. *The Journal of Biological Chemistry*, 298, 102046.
- Zhu, Y., Fan, S., Wang, N., Chen, X., Yang, Y., Lu, Y. et al. (2017) NADPH oxidase 2 inhibitor diphenyleneiodonium enhances ROS-independent bacterial phagocytosis in murine macrophages via activation of the calcium-mediated p38 MAPK signaling pathway. *American Journal of Translational Research*, 9, 3422–3432.

SUPPORTING INFORMATION

Additional supporting information can be found online in the Supporting Information section at the end of this article.

How to cite this article: Fritsch, V. N., Linzner, N., Busche, T., Said, N., Weise, C., Kalinowski, J., Wahl, M. C. & Antelmann, H. (2023). The MerR-family regulator NmlR is involved in the defense against oxidative stress in *Streptococcus pneumoniae*. *Molecular Microbiology*, 119, 191–207. <https://doi.org/10.1111/mmi.14999>